UCRL-11493

University of California

Ernest O. Lawrence Radiation Laboratory

REVIEW OF RECENT WORK ON K^- MESON INTERACTIONS

Berkeley, California

DISCLAIMER

For Conference and Proceedings of
Particle Physics - University of Colorado - Boulder, June 29-July 3, 1964

UCRL-11493

UNIVERSITY OF CALIFORNIA

Lawrence Radiation Laboratory
Berkeley, California

AEC Contract No. W-7405-eng-48

REVIEW OF RECENT WORK ON K^- MESON INTERACTIONS

M. L. Stevenson

June 24, 1964

REVIEW OF RECENT WORK ON K^- MESON INTERACTIONS

M. L. Stevenson

Lawrence Radiation Laboratory
University of California
Berkeley, California

June 24, 1964

I. Introduction

In recent years, ten major bubble chamber exposures have been made to beams of K^- mesons from 0.3 to 5.0 BeV/c. Table I summarizes these exposures in terms of the number of events that would be produced for each millibarn of cross section. (This summary does not include "stopping K^-" runs.) Counter and spark chamber experiments have contributed mainly to total and elastic scattering cross section measurements. Table II summarizes these runs.

The production of new meson and baryon resonances remains the most exciting part of the K^--interaction study. In Section II are summarized the most recent discoveries.

The main purpose of this review is to summarize what is known about the production characteristics of the many outgoing "two-body" channels in the K^--p system. Section III contains this summary.

A summary of the references for each of the reactions is found in Section VIA.

Table I. Bubble chamber exposures.

P_{K^-} (BeV/c)	Total c.m. energy (BeV)	Events/mb (approx)	Chamber	Lab	Date	Groups involved in analysis
0.3-0.8	1.49-1.69	500	15 in. H_2	LRL	1959	LRL
0.6-0.8	1.60-1.69	100	15 in. D_2	LRL	1959	UCLA
0.85-1.15	1.71-1.86	4000	25 in. H_2	LRL	1964	LRL; Univ. Wisconsin
1.15	2.86	800	15 in. H_2	LRL	1958	LRL; UCLA
1.0	1.80	140	72 in. H_2	LRL	1962	LRL
1.1	1.84	220	72 in. H_2			LRL
1.2	1.89	1170	72 in. H_2			LRL
1.3	1.93	1480	72 in. H_2			Univ. Illinois; LRL
1.4	1.98	800	72 in. H_2			LRL
1.5	2.02	5100	72 in. H_2			LRL
1.5	2.02	1000	72 in. D_2			LRL
1.6	2.07	680	72 in. H_2			LRL
1.7	2.11	1070	72 in. H_2			LRL
1.8	2.15	1500	72 in. H_2			UCLA
1.9	2.19	1000	72 in. H_2			UCLA
2.45	2.41	3000	72 in. H_2	LRL	1963-64	LRL
2.55	2.45	6500	72 in. H_2	LRL		LRL
2.64	2.48	8700	72 in. H_2	LRL		LRL
2.64	2.48	6300	72 in. D_2	LRL		LRL
2.70	2.50	5400	72 in. H_2	LRL		Univ. Illinois; LRL
0-0.3	1.43-1.49	100	30 in. D_2	BNL	1964	Univ. Illinois
0.7-1.0	1.65-1.79	200	30 in. H_2	BNL	1964	Univ. Maryland; Naval Res. Lab.
2.0	2.24	200	20 in. H_2	BNL	1962	Univ. Indiana; Iowa State; BNL; Yale; Univ. Colorado; LRL
2.24	2.34	3000	20 in. H_2	BNL	1962-63	BNL; Syracuse
5.0	3.24	1000	80 in. H_2	BNL	1963	BNL
1.47	2.01	200	80 cm H_2	CERN	1963	Zeeman Lab(Amsterdam); Ecole Polytechnique, Saclay
1.47	2.01	1000	30 cm H_2	CERN	1963	CERN; Zeeman Lab; Univ. Glasgow

Table I. (continued)

3.0	2.61	200	80 cm	H_2	CERN 1963	Zeeman Lab; Ecole Polytechnique, Saclay
3.4	2.75		1.15 m	Freon	CERN 1963	Bergen Univ.; CERN; Ecole Polytechnique; Rutherford Lab; University College
3.5	2.78	3000	80 cm	H_2	CERN 1963	Univ. Glasgow; Imperial College; Univ. Oxford; Rutherford Lab.

Table II. Counter and spark chamber experiments.

P_{K^-} (BeV/c)	Detection device	Lab	Comments	Reference
0.63 to 1.1	Counter	LRL	Total K^-p and K^-n cross sections	11
1 to 4	Counter	LRL	Total K^-p and K^-n cross sections	12
0.7 to 1.4	Spark chamber	LRL	K^-p elastic cross sections	17
0.82 to 1.26	Spark chamber	MIT	K^-p elastic cross sections	18
4 to 8	Counter	CERN	K^-p total cross sections	13
2.6 to 3.8	Counter	BNL	K^-p total cross sections	14
4 to 19	Counter	BNL	K^-p total cross sections	15
7.2 to 9	Counter	BNL	K^-p elastic cross sections	16

II. The Production of New Resonant States

Although this is not intended to be a review of all the resonant states, a summary of the properties of known particles and resonant states from the review paper of Rosenfeld, and others* has been included in the Appendix for ready reference. Discussed in this section are the discoveries of the past 6 months.

A. Ω^- Hyperon

The predictions of SU_3[1,2] for the existence of a hyperon, stable to strong decay, of strangeness -3 and mass $\approx$ 1676 MeV, prompted the Brookhaven (BNL) and CERN groups to make extensive exposures at 5.0 and 3.5 BeV/c respectively. The results are now well known. The BNL[3] group, benefiting from higher production energy and the new 80-inch hydrogen chamber, found two remarkable events. The first was an example of the reaction

$$K^- + p \rightarrow \Omega^- + K^+ + K^0, \qquad (2.1)$$

followed by the decay

$$\Omega^- \rightarrow \Xi^0 + \pi^- \qquad (2.2)$$

$$\Xi^0 \rightarrow \Lambda + \pi^0 \qquad (2.3)$$

$$\Lambda \rightarrow p + \pi^-. \qquad (2.4)$$

Furthermore, not one but both of the π^0 γ rays converted! The mass of this Ω^- event was 1680 ± 9 MeV.

The second event[4] was in some respects more unusual than the first one. It was an example of Reaction (2.1), with the Ω^- decaying with low Q value (65 MeV),

---

*Arthur H. Rosenfeld, Angela Barbaro-Galtieri, Walter H. Barkas, P. L. Bastien, Janos Kirz, and Matts Roos, Data on Elementary Particles and Resonant States (UCRL-8030 Part I June 1964 edition) to be published in Rev. Mod. Phys., Oct. 1964.

$$\Omega^- \rightarrow \Lambda + K^- \quad (2.5)$$

$$\Lambda \rightarrow \pi^+ + \pi^- + \pi^- \quad (2.6)$$

$$\Lambda \rightarrow p + \pi^- .$$

The mass for this event was 1674 ± 3 MeV. As of the Washington APS meeting (April 29-30, 1964)[4] no further examples of Reaction (2.1) had been found in the BNL exposure. The cross section for Reaction (2.1) based upon these two events is 2 μb.

The CERN Freon chamber group[5] at 3.4 BeV/c and the CERN H_2 chamber group[41] (British collaboration group) at 3.5 BeV/c both report a negative result and give 3 μb per nucleon as an upper limit to the cross section.

As early as 1954, Eisenberg[6] reported on a cosmic ray event in emulsion that could be an example of yet another mode of decay of the Ω^- with an even lower Q value,

$$\Omega^- \rightarrow \Sigma^0 + K^- . \quad (2.7)$$

Eisenberg stated at the 1964 Washington APS meeting that for this mode of decay, the mass would be 1689^{+10}_{-2} MeV.

It would appear, however, that the mass 1674 ± 3 MeV of the second BNL event with its small error would rule out this possibility, because the sum of the Σ^0 and K^- masses is 1687 MeV, some 13 MeV (> 4 standard deviations) heavier than this event. In any event the Eisenberg particle still remains to be explained.

B. $\Xi^*(1810)$ Hyperon

From the Lawrence Radiation Laboratory (LRL) 2.6- and 2.7-BeV/c exposures[7] has come evidence for the production of an S = -2 hyperon of mass ≈ 1800 MeV. Preliminary evidence was also presented by Halsteinslid et al.[5] The LRL group finds the width of the resonance to be Γ = 70 MeV in the production reaction

$$K^- + p \rightarrow \Xi^*(1810) + K; \qquad (2.8)$$

the decay modes are

$$\Xi^*(1810) \rightarrow \Xi^*(1530) + \pi \qquad (2.9)$$

or

$$\Xi^*(1810) \rightarrow \Lambda + \bar{K}. \qquad (2.10)$$

Even with a limited number of events the LRL group concludes that for the $\Xi^*(1810)$, isospin $T = 1/2$ is highly favored over isospin $T = 3/2$. The cross section is 15 μb.

C. $X^0(960)$ Meson

The Syracuse-BNL group[8] reported evidence for a new meson resonance produced at 2.3 BeV/c in the reaction

$$K^- + p \rightarrow \Lambda + \text{neutrals}. \qquad (2.11)$$

From a missing-mass distribution they were able to identify the two-body reactions

$$K^- + p \rightarrow \Lambda + \pi^0, \qquad (2.12)$$

$$\Lambda + \eta, \qquad (2.13)$$

$$\Lambda + \phi, \qquad (2.14)$$

and a new phenomenon,

$$K^- + p \rightarrow \Lambda + X^0. \qquad (2.15)$$

The X^0 showed itself as a broad peak centered at ≈ 930 MeV.

The LRL group[9] subsequently observed Reaction (2.15) at 2.5, 2.6, and 2.7 BeV/c. In addition to its neutral mode of decay they also observed

$$X^0 \rightarrow \eta + \pi^+ + \pi^-, \qquad (2.16)$$

$$\eta \rightarrow \begin{cases} \pi^+\pi^-\pi^0 \\ \text{or neutrals} \end{cases}. \qquad (2.17)$$

They quote a mass of 959 ± 2 MeV with $\Gamma \leq 12$ MeV. They observed no substantial $\pi^+\pi^-$, $\pi^+\pi^-\pi^0$, $2\pi^+ + 2\pi^-$, $2\pi^+ + 2\pi^- + 2\pi^0$, or $3\pi^+ + 3\pi^-$ decay modes, which implies negligible $n\pi^0$ decay.

The cross section at 2.45 BeV/c (based on 44 events) for the reaction

$$K^- + p \rightarrow \Lambda + (X^0 \rightarrow \eta\pi\pi) \qquad (2.18)$$

is about 40 μb. [The number of 25 μb quoted by Ref. 9 was for $(\Lambda \rightarrow p + \pi^-) + (X^0 \rightarrow \eta\pi\pi)$]. A large fraction of the X^0's is produced with low (momentum transfer)^2 [$-t < 0.5$ (BeV/c)^2].

The BNL group[10] in its continuing study also reported on the decay modes (2.16) and (2.17), and quotes a cross section of ≈ 60 μb based upon ≈ 90 X^0 events at 2.3 BeV/c.

Vigorous work is being continued by both groups to determine the quantum numbers T and J^P.

III. Production Characteristics of K^--Meson Interactions

In the excitement of discovering and identifying the new resonances the production characteristics are often overlooked. It is the purpose of this review to gather together as much information as is possible on the "two-body" final-state channels. When presenting total cross sections we have tried to include all the data available. The angular distributions are presented as isometric figures in an attempt to give an overall view of the energy dependence of the angular distributions. In these it is not always possible to present all the published distributions. There is just too much information to put on a single graph. Selected distributions are presented at appropriate energies.

First a few remarks about kinematics. The invariants s, t, and u are defined as

$$s = (p_1 + q_1 = p_2 + q_2)^2, \qquad (3.1)$$

$$t = (p_1 - p_2 = q_2 - q_1)^2, \qquad (3.2)$$

$$u = (p_1 - q_2 = p_2 - q_1)^2, \qquad (3.3)$$

where q_1 and p_1 are the four-momenta of the K^- and proton, respectively, and q_2 and p_2 the four-momenta of the outgoing meson and baryon, respectively:

$$q_1 = (\omega_1, \vec{q}_1), \qquad q_2 = (\omega_2, \vec{q}_2), \tag{3.4}$$
$$p_1 = (E_1, \vec{p}_1), \qquad p_2 = (E_2, \vec{p}_2),$$

$$p_1^2 = m_1^2, \qquad p_2^2 = m_2^2,$$
$$q_1^2 = \mu_1^2, \qquad q_2^2 = \mu_2^2, \tag{3.5}$$

$$s + t + u = m_1^2 + m_2^2 + \mu_1^2 + \mu_2^2. \tag{3.6}$$

Here μ_1 and m_1 are the rest masses of the K^- and proton, respectively, and μ_2 and m_2 the rest masses of the outgoing meson and baryon, respectively. It is conventional to present the production angular distributions as a function of the cosine of the center-of-mass angle between the incident meson and the outgoing meson, $\cos\theta(\vec{q}_1, \vec{q}_2)$. In this review it will at times be more illustrative to plot the data as a function of ("momentum transfer")^2 = -t.

Since a linear relationship,

$$-t = \omega_1\omega_2 - \mu_2^2 - \mu_1^2 - |\vec{q}_1|\,|\vec{q}_2| \cos\theta(\vec{q}_1, \vec{q}_2), \tag{3.7}$$

exists between (-t) and $\cos\theta(\vec{q}_1, \vec{q}_2)$, these two distributions are equivalent; $s^{1/2}$ is the total energy in the center-of-mass system.

In describing "two-body" production processes it has become fashionable to speak of exchange mechanisms in the s, t, and u channels. The following diagrams symbolize the meanings of the phrases:

(a) "exchange of a particle S in the s channel"

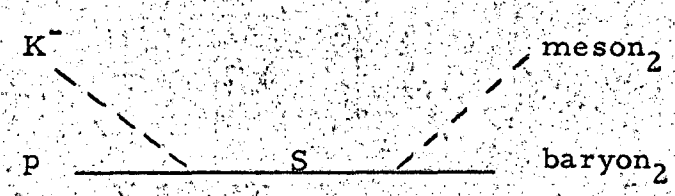

(b) "exchange of particle T in the t channel"

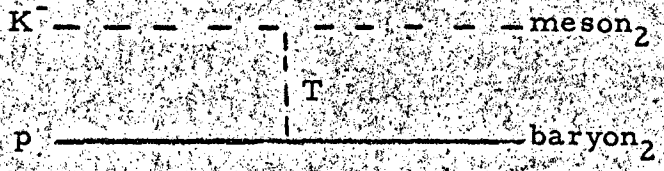

(c) "exchange of a particle U in the u channel"

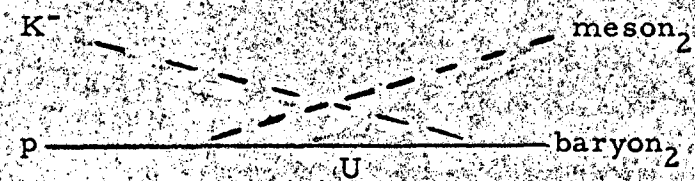

A. Total Cross Sections

Figure 1 summarizes the extensive work that has been done on K^-p and K^-n total cross sections. The data points are too numerous to identify point by point with each research group. The work here comes primarily from counter groups, especially at the higher momenta.

B. $K^- + p \rightarrow K^- + p$

Figures 1 and 2 show the momentum dependence of the total elastic cross section. Figure 3 shows the dependence of $d\sigma/d\Omega$ on the (momentum transfer)^2, $-t$. The data in Fig. 3 are presented on a logarithmic scale to emphasize the character of the diffraction patterns as a function of total energy, $s^{1/2}$. If the forward scattering amplitudes were pure imaginary all distributions would pass through $(4\pi/k\sigma_T)^2 (d\sigma/d\Omega) = 1$ at $-t = 0$. A light line of slope = 7.5 $(BeV/c)^{-2}$ is drawn through this point on all the histograms to aid the eye in comparing the distributions at the different energies. Not all experimental data have been plotted, but only representative samples.

A thorough discussion of diffraction scattering in K^-p interaction will be given by Marshall at this conference. It is not discussed further here.

C. $K^- + p \rightarrow \bar{K}^0 + n$

The momentum dependence of the total cross section for charge-exchange scattering is shown in Figs. 1 and 2. The (momentum-transfer)^2 dependence of the differential cross section is shown in Fig. 4.

The new information shown in this distribution comes from the LRL exposure in the region 1.0 to 1.7 BeV/c[22, 28, 32] and the BNL exposure at 2.0 BeV/c.[31]

Wohl,[22] in the "peak region" of 1 BeV/c, finds evidence for $d_{5/2}$-$f_{5/2}$ interference. At higher momenta (1.4 to 1.7 BeV/c), expansions in Legendre polynomials up to 7th order are required to fit the data.

It is interesting to note how the very pronounced peak at large momentum transfer at $\approx$ 1 BeV/c has diminished and has been replaced by a more diffraction-like peak at 2 BeV/c. This latter phenomenon will be discussed by Marshall. To understand the very sharp backward peaking of charge-exchange scattering will require that the elastic scattering be known well in the same region of maximum momentum transfer. These backward angles play a crucial role in determining the highest-order polynomial required to fit the data. We hope that the spark chamber experiments can be designed to detect in this region. Up to now they have not.

As yet no attempt has been made to fit this charge-exchange scattering by an exchange model. However, it is interesting to note that single-pion exchange cannot occur in the t channel and there are no known S = 1 baryons to be exchanged in the u channel. All this would suggest that T = 0 and T = 1 resonances in the s channel along with ρ exchange in the t channel might play an important role in explaining the charge-exchange data, especially in the region 1 BeV/c ($s^{1/2} \approx$ 1800 MeV).

D. $K^- + p \rightarrow \Xi^- + K^+$

Figure 5 shows the total cross section for $\Xi^- + K^+$ production, with the vertical arrows indicating the thresholds for $\Xi^*(1530) + K$ and $\Xi + K^*(890)$ production. Figure 6 displays the most striking feature of $\Xi^- + K^+$ production, namely, the backward peaking of the K^+. It is not too surprising that large momentum transfer is involved in $\Xi^- + K^+$ production, since there is no known $S = +2$, $Q = 2$ meson that can be exchanged in the t channel.

Polarization information is known over the whole momentum region. Figure 7 summarizes the average polarization as a function of incident momentum. In the region 1.2 to 1.6 BeV/c the polarization generally changes sign at about $\cos \theta_{\Xi}^{c.m.} = 0$.

E. $K^- + p \rightarrow \Xi^0 + K^0$

Figure 8 shows the angular distribution of $\Xi^0 + K^0$ at 1.5 BeV/c. The total cross section is 67 ± 9 μb.

F. $K^- + p \rightarrow \Xi^*(1530) + K$

The total cross section is given in Fig. 9 for the sum of $\Xi^{*0} + K^0$ and $\Xi^{*-} + K^+$.

G. $K^- + p \rightarrow Y_1^*(1385) + \pi$

Figure 10 compares the $Y_1^{*+}(1385) + \pi^-$ total cross section with the $Y_1^-(1385) + \pi^+$ total cross section. It is interesting to note that even though the Y_1^- cannot be formed by K^* exchange whereas the Y_1^+ can, there is an excess of Y_1^- over Y_1^+ up to ≈ 1.5 BeV/c. By 2.0 BeV/c there is little or no evidence for Y_1^-, whereas there are still observable amounts of Y_1^+.

Figures 11 and 12 display the (momentum-transfer)^2 distributions for $Y_1^{*+} + \pi^-$ and $Y_1^{*-} + \pi^+$, respectively.

Cooper et al.[45] suggested at Sienna that because the angular distributions for Y_1^+ and Y_1^- at 1.45 BeV/c are so similar K^* exchange is not playing a dominant role in Y_1^+ production. It is interesting to note that one of the few exchange mechanisms these two reactions have in common is the exchange of the N_{33}^* in the u channel. Perhaps at low incident momenta this process plays an important role. The exchange of a nucleon (neutron) in Y_1^- production, which is not possible for Y_1^+ production, may account in part for the excess of Y_1^- over Y_1^+ below 1.5 BeV/c.

H. $K^- + p \rightarrow \Sigma^{\pm} + \pi^{\mp}$

Here in Fig. 13, which displays the total cross section, we see two of the major final-state channels at low energy become two minor ones at high energy. In particular, the Σ^- production, which cannot benefit from K^* exchange in the t channel, falls substantially below that of Σ^+, which can.

The angular distributions or $(\text{momentum-transfer})^2$ distributions of Figs. 14 and 15 show at higher momenta[41, 46] that the production mechanisms for Σ^+ and Σ^- are drastically different.

I. $K^- + p \rightarrow K^{*-} + p$

The total cross section for this reaction is given in Fig. 16, and the limited information on the angular distribution for K^* production is given in Fig. 17.

J. $K^- + p \rightarrow \Lambda + \phi$

Figure 18 gives the total cross section and Fig. 19 the angular distributions. We hope that more will be reported on this very interesting reaction as the data from the recent BNL, CERN, and LRL exposures are analyzed.

K. $K^- + p \rightarrow \Lambda + \rho$

The measurement of this process is made difficult because it is of the

same topology as $K^- + p \rightarrow Y^*(1385) + \pi$, a reaction that seems to dominate the $\Lambda\pi^+\pi^-$ final state. Figure 20 summarizes what is known of the total cross section. Little is reported on the production angular distributions.

L. $K^- + p \rightarrow \Lambda + \omega$

This is a reaction that has intrigued us[60] for some time. It is readily identifiable, a pure $T = 0$ final state, with a vector meson whose decay can be correlated with various suitable directions in the production process and with the Λ spin. A preliminary analysis of the decay density-matrix has clearly shown that K and K^* exchange in the t channel alone cannot explain the existence of certain large density-matrix elements. All the events of the type $K^- + p \rightarrow \Lambda + \pi^+\pi^-\pi^0$ are being measured in the LRL 1.2- to 1.7-BeV/c exposure to better determine these matrix elements as a function of both s and t.

Figure 21 displays the energy variation of the total cross section for $K^- + p \rightarrow \Lambda + (\omega \rightarrow \pi^+\pi^-\pi^0)$. The $(\text{momentum-transfer})^2$ dependence of the differential cross section is shown in Fig. 22. The positions of the poles in the t channel at $t = M_K^2$ and $t = M_{K^*}^2$ are shown as solid straight lines to the left of the physical region, and the pole at $u = M_p^2$ is shown as a solid straight line to the right of the physical region. If there is a Regge recurrence of the $Y_0(1405)$ it should occur at about $S = 4\ (\text{BeV})^2$. If such a state exists, it is not conspicuous in the $K^- p \rightarrow \Lambda\omega$ total cross section or the production angular distribution.

M. $K^- + p \rightarrow \Lambda + \pi^0$

The $\Lambda\pi^0$ final state is identified by looking at the $(\text{missing mass})^2$ distribution in the $K^- + p \rightarrow \Lambda +$ neutral topology. Figure 23 displays these distributions for several incident K momenta. These distributions are not

normalized, and are presented only to show the π^0 peak near $(0.135\ \text{BeV})^2$, the η peak near $(0.55\ \text{BeV})^2$, and the "$\omega \rightarrow$ neutral" peak at $(0.79\ \text{BeV})^2$. The position of $(M_{X^0} = 0.959)^2$ occurs at the very end of the 1.7-BeV/c distribution. The (MM) resolution function increases by a factor of 4 from low momentum transfer to high momentum transfer. This makes the identification of the $\Lambda + \pi^0$ final state difficult near $(-t)_{max}$. However, it appears that there is not much "background contamination" in this region, so that the difficulties are minimized.

If there is a Regge recurrence of the $Y_1^*(1385)$, it, like the $Y_0^*(1405)$, should have a mass of $s^{1/2} \approx 2$ BeV. We have looked for an enhancement in the pure $T = 1$ $(K^- + p \rightarrow \Lambda + \pi^0)$ total cross section at $s^{1/2} = 2$ BeV (or $P_{K^-} \approx 1.5$ BeV/c). Figure 24 shows that if such a recurrence exists it is not evident in the total cross section. Figure 25 displays the (momentum-transfer)^2 distribution of $\Lambda\pi^0$ as a function of incident lab momentum. Here again we plot as solid lines the positions of the K^* pole in the t channel at $t = M_{K^*}^2$ and of the proton pole in the u channel at $u = M_p^2$.

The Λ polarization, though rather poorly known because of limited statistics, is summarized in Fig. 26.

We have made our first attempt to understand the moderate-energy K^--p interaction (i.e., $0.6\ \text{BeV/c} < P_{K\ \text{lab}} < 1.7\ \text{BeV/c}$) by attempting to fit the differential cross section and the Λ polarization with an exchange model. Our approach is similar to those of others[66-67] who have studied the "associated production" reaction $\pi^- + p \rightarrow \Lambda + K^0$.

The following diagrams summarize the Born terms that arise from the exchanged particles in the s, t, and u channels.

Born Terms

s channel:

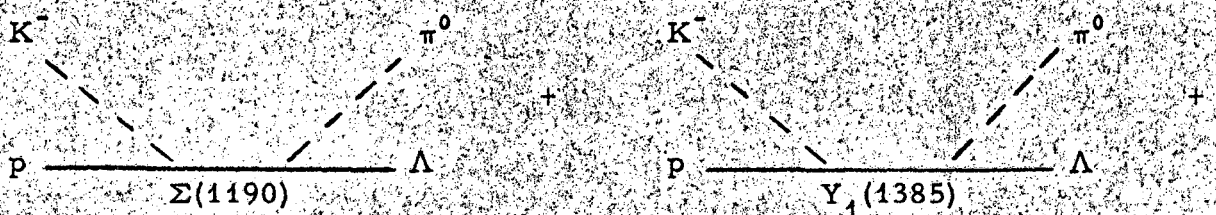

t channel:

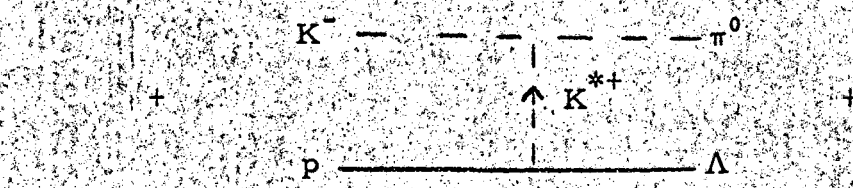

u channel:

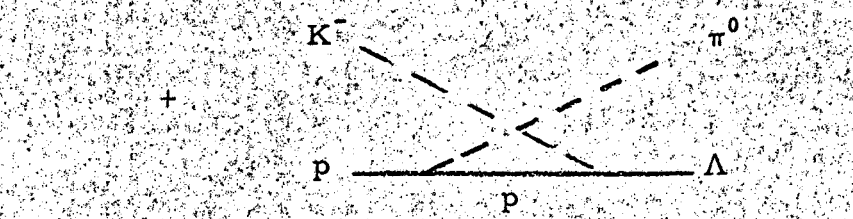

Since the Born terms are all relatively real (by time-reversal invariance),[67] they alone cannot produce any Λ polarization. Resonance terms of a Breit-Wigner form are introduced into the s channel at the masses of known or expected resonances. The Λ polarization arises from interference with these terms. In a preliminary study we have introduced the following resonances into the s channel:

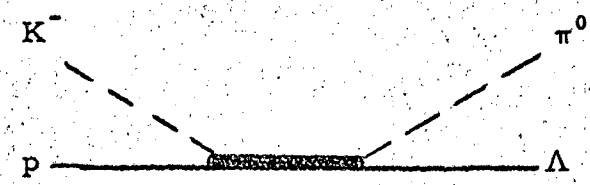

$P_{3/2}(1660)$,

$D_{5/2}(1765)$,

$F_{5/2}(1920)$ (possible Σ recurrence),

$F_{7/2}(2030)$ (possible $Y_1(1385)$ recurrence).

The widths of the 1660 and 1765 were fixed at their experimental values. Eleven parameters in all were used, one for Σ exchange, one for $Y_1^*(1385)$, two for K^*, one for the proton, one for the $P_{3/2}(1660)$ resonance, one for $D_{5/2}(1765)$, two for $F_{5/2}(1920)$, and two for $F_{7/2}(2030)$.

Figures 27, 28, and 29 show how one particular solution fits the data over the region 0.62 BeV/c to 1.70 BeV/c. At this stage no claim is made that the model and reality have anything to do with each other. This type of analysis is premature because the quantum numbers of the $Y_1(1660)$ and Y(1765) are not known yet, and it seems very doubtful that this sort of analysis could be used to determine them. Furthermore, it is our belief that a more sophisticated model is required, one that takes into account the strong absorption that must occur for small impact parameters or large momentum transfer. Perhaps an approach similar to Ross and Shaw[70] and Gottfried and Jackson[71] will help improve the fit to the data once the $Y_1(1660)$ and Y(1765) quantum numbers are known.

N. Other "Two-Body" Processes

Lack of time has prevented us from discussing other two-body processes such as

$$K^- + p \rightarrow \Sigma^0 + \pi^0,$$

$$K^- + p \rightarrow \Lambda + \eta,$$

$$K^- + p \rightarrow Y_0^*(1520) + \pi,$$

$$K^- + p \rightarrow Y_1(1660) + \pi,$$

and

$$K^- + p \rightarrow Y_1(1765) + \pi.$$

The new data from LRL on reactions such as

$$K^- + p \rightarrow Y_1^*(1385) + \rho$$

and other "double resonance" reactions in the 2- to 3-BeV/c exposures are not in publishable form as yet, and hence are not presented here.

IV. Conclusions

The manner in which most of the two-body production processes rise from threshold, reach a maximum value, and steadily fall suggests that competition among the many channels plays a major role in the production process. Models that do not take this into account are likely to fail. To think of the production processes in terms of exchange mechanisms alone is too naive.

Perhaps a more realistic picture of the nucleon as the high-energy K^- sees it is as a peripheral annular ring plus a central disk. In the peripheral part, exchanges in the t channels dominate and give rise to the peaking at low momentum transfer. What goes on in the central disk might be treated by a statistical model, much as has been done in antiproton-proton annihilation. Whatever the model is, one experimental trend seems clear. Events of any given "two-body" process are becoming rarer. Those that are most interesting usually involve particles with high mass and quite often high spin. A complete analysis involves the decay correlation matrix. The matrix elements require large numbers of events for their determination. If the study of the production mechanisms is to be pursued seriously, then the bubble chamber exposures

must be made much larger than they have been and the data-processing systems increased in speed by at least an order of magnitude. Meanwhile, as was stated in the introduction, the most exciting thing now is the discovery and identification of new resonant states. The filling in of the Mendeléev table of elementary particles is more interesting than the chemistry at the moment.

ACKNOWLEDGMENTS

We have received generous assistance from Charles Wohl in preparing this summary. We express our thanks to him and to Richard Hubbard and Darrell Huwe for allowing some of the results of their thesis work to be reported at this conference.

This work was done under the auspices of the U. S. Atomic Energy Commission.

REFERENCES

The following journal abbreviations are used in the references.

PR	= Physical Review
PRL	= Physical Review Letters
'62 CERN	= 1962 International Conference on High Energy Physics at CERN
'63 Sienna	= Proceedings of the Sienna International Conference on Elementary Particles (Società Italiana di Fisica, Bologna, 1963)
BAPS	= Bulletin American Physical Society
NC	= Il Nuovo Cimento
UCRL	= Lawrence Radiation Laboratory Report
NP	= Nuclear Physics

1. M. Gell-Mann, PR 125, 1067 (1962).
2. Y. Ne'eman, NP 26, 222 (1961).
3. Barnes et al., PRL 12, 204 (1964).
4. N. Samios, BAPS 9, 482 (1964) (Wash).
5. Halsteinslid et al., '63 Sienna, 173.
6. Y. Eisenberg, PR 96, 541 (1954).
7. Smith et al., UCRL-11456 (submitted to PRL).
8. Goldberg et al., BAPS 9, 23 (1964) (NY).
9. Kalbfleisch et al., PRL 12, 527 (1964).
10. Goldberg et al., PRL 12, 546 (1964).
11. Chamberlain et al., PR 125, 1696 (1962).
12. Cook et al., PR 123, 320 (1961).
13. von Dardel et al., PRL 5, 333 (1960).
14. Baker et al., '63 Sienna, 634.

15. Baker et al., PR 129, 2285 (1963).

16. Foley et al., PRL 11, 503 (1963).

17. Beall et al., '62 CERN, 368.

18. Sodickson et al., PR 133, B757 (1964).

19. W. Humphrey and R. Ross, PR 127, 1305 (1962).

20. Watson et al., PR 131, 2248 (1963).

21. P. Bastien and P. Berge, PRL 10, 188 (1962).

22. C. Wohl and S. Wojcicki, UCRL-11340 (in preparation) and C. Wohl, K^-p Interactions near 1070 MeV/c: Hyperon Channels; (Thesis) UCRL-11528.

23. W. Graziano and S. Wojcicki, PR 128, 1868 (1962).

24. J. Munson, K^-p Elastic Scattering at 1.22 BeV/c,(Thesis) UCRL-11155, Dec. 1963 (unpublished).

25. Crittenden et al., PRL 12, 429 (1964).

26. Swanson et al., BAPS 8, 602 (1963).

27. Ferro-Luzzi et al., '62 CERN, 376.

28. Wohl et al., BAPS 9, 442 (1964).

29. Buschbeck et al., '63 Sienna, 166.

30. P. Dauber, PR 134, 1370 (1964).

31. Barge et al., PRL 13, 69 (1964).

32. R. Hulsizer (private communication) and BAPS 9, 33 (1964).

33. C. Wohl, K^-p Interactions near 1070 MeV/c:Hyperon Channels, (Thesis) UCRL-11528, June 1964.

34. Bertanza et al., '62 CERN, 284.

35. Trower et al., BAPS 9, 33 (1964).

36. P. Bastien, K^--Proton Interactions Near 760 MeV/c, (Thesis) UCRL-10779, Feb. 1963.

37. Alvarez et al., '62 CERN, 433, and Berge et al., UCRL-11529 (to be submitted to PR).

38. R. Hubbard, Properties of Neutral Cascade Hyperons (Thesis), UCRL-11510.

39. Bertanza et al., '62 CERN, 284.

40. Ticho et al., '62 CERN, 436.

41. Blair et al., '63 Sienna, 146.

42. Chu et al., BAPS 9, 441 (1964).

43. Gelsema et al., '63 Sienna, 143.

44. R. Hubbard, Properties of the Neutral Cascade (Thesis), UCRL-11510.

45. Cooper et al., '63 Sienna, 162.

46. Gelsema et al., '63 Sienna, 134.

47. D. Huwe, Study of the Reaction $K^- + p \rightarrow \Lambda + \pi^+ + \pi^-$ from 1.2 to 1.7 BeV/c (Thesis), UCRL-11291.

48. Bastien et al., '62 CERN, 373.

49. P. Bastien and J. P. Berge, PRL 10, 188 (1963).

50. Barge et al., BAPS 9, 431 (1964).

51. Bertanza et al., PRL 10, 176 (1963).

52. Barbaro-Galtieri et al., BAPS 9, 23 (1964).

53. Cooper et al., '62 CERN, 301.

54. Cooper et al., '63 Sienna, 154.

55. S. Wojcicki, UCRL-11138 (to be published in PR).

56. Alston et al., '62 CERN, 291.

57. Gelsema et al., '63 Sienna, 170.

58. Connolly et al., '63 Sienna, 130.

59. Schlein et al., PRL 10, 368 (1963).

60. Flatte et al., BAPS 8, 603 (1963).

61. S. Berman and R. Oakes, Angular Correlations in Production Processes, (to be published in PR).

62. R. Huff, BAPS 8, 604 (1963).

63. N. Byers and C. N. Yang, Phenomenological Analysis of Reactions such as $K^- + p \rightarrow \Lambda + \omega$, (submitted for publication).

64. Ferro-Luzzi et al., PRL 8, 28 (1962).

65. Stevenson et al., BAPS 9, 441 (1964).

66. M. Gourdin and M. Rimpault, NC 20, 1166 (1961).

67. A. Kanazawa, PR 123, 997, (1961).

68. MacDowell et al., NP 31, 636 (1962).

69. G. T. Hoff, PR 131, 1302 (1963).

70. M. Ross and G. Shaw, PRL 12, 627 (1964).

71. K. Gottfried and J. D. Jackson, Influence of Absorption Due to Competing Processes on Peripheral Reactions (to be published).

Appendix A. References to Specific Reactions

1. New resonant states

   Refs. 1 through 10.

2. Total cross sections

   Refs. 11 through 15.

3. Elastic scattering

   Refs. 16 through 26.

4. Charge-exchange scattering

   Refs. 19 through 22, 27 through 36.

5. Cascade hyperon production

   Refs. 37 through 44.

6. $K^- + p \rightarrow Y_1^*(1385) + \pi$

   Refs. 22, 41, 45 through 51.

7. $K^- + p \rightarrow \Sigma^{\pm} + \pi^{\mp}$

   Refs. 23, 36, 41, 46, 48, 52 through 54.

8. $K^- + p \rightarrow K^{*-} + p$

   Refs. 39, 46, 49, 55 through 57.

9. $K^- + p \rightarrow \Lambda + \phi$

   Refs. 41, 43, 58, 59.

10. $K^- + p \rightarrow \Lambda + \rho$

    Refs. 46, 47.

11. $K^- + p \rightarrow \Lambda + \omega$

    Ref. 46, 58, 60 through 63.

12. $K^- + p \rightarrow \Lambda + \pi^0$

    Refs. 32, 36, 48, 64, 65.

13. Theory of Production Mechanisms

    Refs. 66 through 71.

Appendix B. Tables from Rosenfeld et al.*

Table S - Stable particles

						Important decays			
	$I(J^{PG})CA$	Mass (MeV)	Mass diff. (MeV)	Mean life (sec)	$Mass^2$ $(BeV)^2$	Partial mode	Fraction	Q (MeV)	p or p_{max} (MeV/c)
LEPTONS									
γ	$J^P=1^-C^-A^+_?$	0		stable	0	stable			
ν_e	J=1/2	0(<0.2 keV)		stable	0	stable			
ν_μ		0(<4 MeV)			0				
$e^\pm$	J=1/2	0.511006 ±0.000002		stable	0.000	stable			
$\mu^\pm$	J=1/2	105.659 ±0.002	-33.95 ±0.05	2.2001×10^{-6} ±.0008 ×scale=2.5	0.011	$e\nu\nu$	100%	105.66	52.8
MESONS									
$\pi^\pm$	$1(0^{--})C^+_nA^-_?$	139.60 ±0.05		2.55×10^{-8} ±.26	0.019	$\mu\nu$	100%	33.95	29.80
						$e\nu$	$(1.24\pm.05)10^{-4}$	139.60	69.80
						$\mu\nu\gamma$	$(1.24\pm.25)10^{-4}$	33.94	29.81
						$\pi^0e\nu$	$(1.5\pm.3)10^{-8}$	4.08	4.49
π^0		135.01 ±0.05	4.590 ±.004 ×scale=2.4	1.80×10^{-16} ±.29 ×scale=1.3	0.018	$\gamma\gamma$	100%	135.01	67.51
$K^\pm$	$1/2(0^-)A^-_?$	493.8 ±0.2		1.229×10^{-8} ±.008	0.244	$\mu\nu$	(63.1±.4)%	388.1	235.6
						$\pi^\pm\pi^0$	(21.5±.4)%	219.2	205.2
						$\pi^\pm\pi^-\pi^+$	(5.5±.1)%	75.0	125.5
						For other decays see Table S Decays			
K^0		498.0 ±0.5	-4.2 ±0.5 ×scale=1.2	50% K1, 50%K2					
K_1				0.92×10^{-10} ±.02	0.248	$\pi^+\pi^-$	(69.4±5.1)%	218.8	206.2
						$\pi^0\pi^0$	(30.6±1.1)%	228.0	209.2
K_2			$-0.91\times1/\tau_1$ ±0.07 ×scale=2.3	5.62×10^{-8} ±.68	0.248	$\pi^0\pi^0\pi^0$	(27.1±3.6)%	93.0	139.5
						$\pi^+\pi^-\pi^0$	(12.7±1.7)%	83.8	133.1
						$\pi\mu\nu$	(26.6±3.2)%	252.7	216.2
						$\pi e\nu$	(33.6±3.3)%	357.9	229.4
η	$0(0^{-+})C^+A^-_?$	548.7 ±0.5		$\Gamma<10$ MeV	0.301	$\gamma\gamma$	(35.3±3.0)%	548.7	274.4
						$3\pi^0$ or $\pi^02\gamma$	(31.8±2.3)%	143.7	179.4
						$\pi^+\pi^-\pi^0$	(27.4±2.5)%	134.5	174.4
						$\pi^+\pi^-\gamma$	(5.5±1.3)% ×scale=1.1	269.5	236.2
BARYONS									
p	$1/2(1/2^+)$	938.256 ±0.005	-1.2933 ±.0001	stable	0.880				
n		939.550 ±0.005		1.01×10^3 ±.03	0.883	$pe^-\nu$	100%	0.78	1.19
Λ	$1/2(1/2^+)$	1115.40 ±0.11		2.62×10^{-10} ±.02 ×scale=1.5	1.244	$p\pi^-$	(67.7±1.0)% ×scale=1.2	37.5	100.2
						$n\pi^0$	(31.6±2.6)%	40.9	103.6
						$p\mu\nu$	$<1\times10^{-4}$	71.5	130.7
						$pe\nu$	$(.88\pm.08)10^{-3}$ ×scale=1.7	176.6	163.1
Σ^+	$1/2(1/2^+)$	1189.41 ±0.14		0.788×10^{-10} ±.027	1.415	$p\pi^0$	51.0±2.4%	116.13	189.03
						$n\pi^+$	49.0±2.4%	110.26	185.06
						For other decays see Table S Decays			
Σ^0		1192.4 ±0.3 ×scale=1.4	4.44 ±.10	$<1.0\times10^{-14}$	1.422	$\Lambda\gamma$	100%	77.0	74.5
Σ^-		1197.08 ±0.19		1.58×10^{-10}	1.433	$n\pi^-$	100%	116.94	191.73
						For other decays see Table S Decay			
Ξ^0	$1/2(1/2^+)$?	1314.3 ±1.0	6.5 ±1.0	3.06×10^{-10} ±.40 ×scale=1.2	1.727	$\Lambda\pi^0$	100%	76.9	150.1
						For other decays see Table S Decay			
Ξ^-		1320.8 ±0.2 ×scale=1.3		1.74×10^{-10} ±.05	1.745	$\Lambda\pi^-$	100%	65.8	138.7
						$\Lambda e^-\nu$	$(3.0\pm1.7)10^{-3}$	204.9	189.4
						$n\pi^-$	$<5\times10^{-3}$	214.7	303.0
Ω^-	$0(3/2^+)$? ?	1675 ±3		$\sim0.7\times10^{-10}$		$\Xi\pi$	?	221	296
						ΛK	?	66	216

* A. H. Rosenfeld, A. Barbaro-Galtieri, W. H. Barkas, P. L. Bastien, J. Kirz, M. Roos UCRL-8030 - Part I. June 1964.

Table S Decay

An Appendix to Table S for particles with many decay modes

	Partial mode	Rate		Q (MeV)	p or p_{max} (MeV/c)
$K^{\pm}$	$\mu^{\pm}\nu$	63.1±.5%	} X scale=1.6	388.1	235.6
	$\pi^{\pm}\pi^{0}$	21.5±.4%		219.2	205.2
	$\pi^{\pm}\pi^{+}\pi^{-}$	5.5±.1%		75.0	125.5
	$\pi^{\pm}\pi^{0}\pi^{0}$	1.7±.1%		84.2	133.0
	$\pi^{0}\mu^{\pm}\nu$	3.4±.2%		253.1	215.2
	$\pi^{0}e^{\pm}\nu$	4.8±.2%		358.3	228.4
	$\pi^{\pm}\pi^{\mp}e^{\pm}\nu$	$(4.3\pm.9)10^{-5}$		214.1	203.5
	$\pi^{\pm}\pi^{\pm}e^{\mp}\nu$	$<0.1\times10^{-5}$		214.1	203.5
Σ^{+}	$p\pi^{0}$	(51.0±2.4)%		116.1	189.0
	$n\pi^{+}$	(49.0±2.4)%		110.3	185.1
	$n\pi^{+}\gamma$	$\sim0.4\times10^{-4}$		110.3	185.1
	$\Lambda e^{+}\nu$	$\sim0.2\times10^{-4}$		73.5	71.7
	$p\gamma$	$\sim3\times10^{-3}$		251.1	224.6
	$n\mu^{+}\nu$	$<2.3\times10^{-4}$		144.2	202.4
	$ne^{+}\nu$	$<1.0\times10^{-4}$		249.3	223.6
Σ^{-}	$n\pi^{-}$	100%		117.9	192.7
	$n\pi^{-}\gamma$	$\sim0.1\times10^{-4}$		117.9	192.7
	$n\mu^{-}\nu$	$(0.66\pm0.14)10^{-3}$		151.9	209.3
	$ne^{-}\nu$	$(1.4\pm0.3)10^{-3}$		257.0	229.8
	$\Lambda e^{-}\nu$	$(0.75\pm0.28)10^{-4}$		81.2	78.9
Ξ^{0}	$\Lambda\pi^{0}$	~ 100%		76.9	150.1
	$p\pi^{-}$	<0.4%		249.4	309.3
	$pe^{-}\nu$	<0.4%		388.5	332.0
	$\Sigma^{+}e^{-}\nu$	<0.3%		137.4	130.7
	$\Sigma^{-}e^{+}\nu$	<0.25%		129.7	123.8

A. H. Rosenfeld, A. Barbaro-Galtieri, W. H. Barkas, P. L. Bastien, J. Kirz, M. Roos
UCRL-8030 - Part I. June 1964.

Baryons

		Beam πp(MeV) or kp(MeV)	I(J^P) ⊢=estab.	Sym-bol	Mass (MeV)	Γ (MeV)	Mass² (BeV)²	Important Decays: Partial mode	Fraction (%)	Q (MeV)	p or pmax (MeV)
N	p		1/2(1/2+)	N_a	938.2		0.88	See table S			
	n				939.6		0.88				
	$N^*_{1/2}(1480)$	550 πp (MeV)	1/2(1/2+)	N_a	~1480	~240	2.19	πN	~50	402	426
	$N^*_{1/2}(1512)$	600 πp	1/2(3/2−)	N_γ	1518 ± 10	125 ±12	2.30	πN	~80	440	454
								Nππ		301	408
	$N^*_{1/2}(1688)$	900 πp	1/2(5/2+)	N^{II}_a	1688	100	2.85	πN	~80	610	572
								Nππ		471	538
	$N^*_{1/2}(2190)$	1935 πp	1/2(9/2+)	N^{III}_a	2190	~200	4.80	πN	~30	1112	888
								Λk		577	710
	$N^*_{1/2}(2700)$	3265 πp	1/2	N	2700	~100	7.29	ηN	large	1213	1115
								πN	~6	1622	1182
Δ	$N^*_{3/2}(1238)$	198 πp	3/2(3/2+)	Δ_δ	1236 ± 2	125	1.53	πN	100	160	233
	$N^*_{3/2}(1920)$	1347 πp	3/2(7/2+)	Δ^{II}_δ	1924	170	3.70	πN	34	842	722
								ΣK		237	430
	$N^*_{3/2}(2360)$	2350 πp	3/2(11/2+)	Δ^{III}_δ	2360	~200	5.57	πN	~10	1282	988
Λ	Λ		0(1/2+)	Λ_a	1115.4		1.24	See table S			
	$Y^*_0(1405)$	<0 Kp	0(1/2−)	Λ_β	1405	50	1.97	Σπ	100	76	151
								Λππ	< 1	10	69
	$Y^*_0(1520)$	Kp 395 (MeV/c)	0(3/2−)	Λ_γ	1518.9 ±1.5	16 ±2	2.31	Σπ	55±7	190	266
								K̄N	29±4	87	243
								Λππ	16±2	124	251
	$Y^*_0(1815)$	1040 Kp	0(5/2+)	Λ^{II}_a	1815	70	3.29	K̄N	80	875	664
								Σπ	<10	486	504
								Λππ	<15	420	515
								Λη	?	151	344
Σ	Σ	<0 Kp	1(1/2+)	Σ_a	+1189.4		1.41	See table S			
					-1197.1		1.43				
					1192.4		1.42				
	$Y^*_1(1385)$	<0 Kp	1 3/2+	Σ_δ	1382.1 ±.9	53 ±2	1.91	Λπ	96±4	127	205
					×scale=1.5	×scale=2.4		Σπ	4±4	55	124
	$Y^*_1(1660)$	715 Kp	1 ( )	Σ	1660 ±10	44 ±5	2.76	K̄N	~5	720	564
								Σπ	~31	328	383
								Λπ	~21	405	439
								Σππ	~27	188	321
								Λππ	~16	265	389
	$Y^*_1(1765)$	940 Kp	1(5/2−)	Σ	1765 ±10	60 ±10	3.12	K̄N	60	825	632
								Λπ		510	517
								Σπ, Λππ	Not yet resolved from $Y^*_0(1815)$		
	Only recently resolved from $Y^*_0(1815)$										
Ξ	Ξ		1/2(1/2+)	Ξ_a	-1321		1.75	See table S			
					1314		1.73				
	$\Xi^*(1530)$		1/2(3/2+) p wave	Ξ_δ	1529.1 ±1.0	7.5 ±1.7	2.34	Ξπ	~100	73	148
	$\Xi^*(1810)$		1/2( )	Ξ	1810 ±20	~70	3.27	$\Xi^*\pi$	~45	141	225
								ΛK̄	~45	197	386
								Ξπ	<10	354	406
								ΣK̄	<10	127	307
Ω	$\Omega^-(1675)$		0(3/2+)	Ω_δ	1675 ±3		2.81	See table S			

A. H. Rosenfeld, A. Barbaro-Galtieri, W. H. Barkas, P. L. Bastien, J. Kirz, M. Roos
UCRL-8030 - Part I. June 1964.

Mesons

						Important decays			
	Mass (MeV)	$I(J^{PG})CA$ ⟷ = estab.	Symb.	Γ (MeV)	M^2 (BeV^2)	Partial modes	Fraction %	Q (MeV)	p or p_{max} (MeV/c)
η	548.7 ±0.5	$0(0^{-+})C^+A^-$ ⟷	η_β	<10	0.301	See table S			
ω	782.8 ±0.5	$0(1^{--})C^-A^-$ ⟷	η_γ	9.4 ±1.7	0.613	$\pi^+\pi^-\pi^0$	86	369	327
	×scale = 1.8					$\pi^+\pi^-$	<1	504	366
						neutral($\pi^0\gamma$)	11±1	648	380
						$\pi^+\pi^-\gamma$	3.2±1	504	366
						e^+e^-	<0.3	782	391
						$\mu^+\mu^-$	<0.5	572	377
η2π	959 ±2	$0(0^{-+},1^{++},\ldots)C^+A^-$ η		<12	0.920	η2π	large	131	232
						2π	<20	680	459
		Conceivably strongly decaying $1(J^{P+})C^-$ or electromagnetic decay of G=-1 meson				3π	<30	540	427
						4π	< 3	400	372
						6π	< 3	121	189
						ππγ	?	680	459
K_1K_1	~1000	May be just large $\bar{K}K$ scattering length, see listings of data cards.							
φ	1019.5 ±0.3	$0(1^{--})C^-A^+$ ⟷	η_γ	3.1 ±0.6	1.040	K_1K_2	41±6	23	109
	×scale = 1.7					K^+K^-	59±6	32	126
						ππ	<8	740	490
		Suppressed by A=+1 approximation				$\pi\rho+3\pi$	<10	117	188
						$\pi\delta\gamma$		885	501
f	1253 ±20	$0(2^{++})C^+A^+$	η_a^{II}	100 ±25	1.571	ππ	large	974	611
						4π	8±6	695	547
						$\bar{K}K$	?	265	386
$\bar{K}K\pi$	1410	$\leq 1(0^{-+},1^{++},\ldots)C^+A^-$ η ⟷		60		$K^*\bar{K}$	large	25	126
						$K\bar{K}\pi$	small	283	421
		If we guess I=0, then G=+1				2π	?	1131	691
		Could be Peierls mechanism				$\bar{K}K$	?	422	503
						3π	?	991	670
$\pi^\pm$	139.6	$1(0^{--})C_n^+A^-$	π_β			See table S			
π^0	135.0	⟷							
ρ	763 ±4	$1(1^{-+})C_n^-A^+$ ⟷	π_γ	106 ±5	0.582	2π	100	483	355
						4π	small	204	241
A1	1090 ±?	$\geq 1(0^{--})C_nA^-$ ⟷ ?	π	125 ±25		ρπ	~100	188	251
						$\bar{K}K$	<5	G- forbidden for odd ℓ if I=1	
	May be just large ρπ scattering length								
	Only recently separated from A2; could be Peierls mechanism								
B	1215 ±18	$1(1^{++},2^{-})C_n^-A^+$ ⟷ ⟷ ⟷	π_δ	122 ±17	1.476	ωπ	~100	293	335
						ππ	<30	I forbidden for even ℓ	
				×scale = 1.9		$\bar{K}K$	<10	G forbidden for even ℓ	
						4π	<50	657	525
A2	1310	$1(2^{+-})C_n^+A^?$ ⟷	π_a^{II}	80		ρπ	~70	408	418
						$\bar{K}K$	~30±7	816	562
	Only recently separated from A1(1090)					ηπ	seen	622	529
$K^\pm$	493.8	$1/2(0^-)$ A^-	K_β		0.244	See table S			
K^0	498.0	⟷							
kappa	725	Seen weakly in occasional experiments							
K^*	891 ±1	$1/2(1^-)A^+$ ⟷	K_γ	50 ±2	0.794	Kπ	~100	258	288
				×scale=1.3		Kππ	<0.2	118	215
						κπ	<0.2	27	82
K_C	1215 ±15	$\leq 3/2(1^+)A^-$ ⟷ ? ?	K	60 ±10	1.476	Kρ	strong	-30	<0
						$K^*\pi$	?	184	253
	Could be Peierls mechanism								

A. H. Rosenfeld, A. Barbaro-Galtieri, W. H. Barkas, P. L. Bastien, J. Kirz, M. Roos UCRL-8030 - Part I. June 1964.

Figure Legends

Fig. 1. Total cross sections. Refs. 11 - 15.

Fig. 2. Total elastic scattering and charge-exchange scattering cross sections in the region 0.1 to 2.5 BeV/c. Elastic scattering, Refs. 16-26; charge exchange, Refs. 27-35.

Fig. 3. $K^- + p \rightarrow K^- + p$ differential cross section.

7.2 and 9.0 BeV/c, Foley et al., Ref. 16;
2.0 BeV/c, Crittenden et al., Ref. 26;
1.4 BeV/c, Beall et al., Ref. 17;
1.22 BeV/c, Munson, Ref. 24.

Also see Appendix A3.

Fig. 4. $K^- + p \rightarrow \bar{K}^0 + n$ differential cross section.

2.0 BeV/c, Barge et al., Ref. 31;
1.8 BeV/c, Dauber, Ref. 30;
1.4 to 1.7 BeV/c, Wohl et al., Ref. 28;
1.34 BeV/c, Trower et al., Ref. 35;
1.22 BeV/c, Ferro-Luzzi et al., Ref. 27;
1.025 to 1.125 BeV/c, Wohl, Ref. 33, 22;
0.85 BeV/c, Bastien, Ref. 36.

Also see Appendix A4.

Fig. 5. $K^- + p \rightarrow \Xi^- + K^+$ total cross section.

Refs. 37-43.

Fig. 6. $K^- + p \rightarrow \Xi^- + K^+$ angular distributions.

1.2 to 1.7 BeV/c, Alvarez et al., Ref. 37;
1.8 BeV/c, Ticho et al., Ref. 40;
2.2 BeV/c, Bertanza et al., Ref. 39.

Fig. 7. Average Ξ^- polarization.

Refs. 37, 39, 40.

Fig. 8. $K^- + p \rightarrow \Xi^0 + K^0$ angular distribution.

Ref. 38.

Fig. 9. $K^- + p \rightarrow \Xi^*(1530) + K$ total cross section.

Refs. 37, 39-41, 43.

Fig. 10. $K^- + p \rightarrow Y_1^*(1385) + \pi$ total cross section.

Refs. 41, 45-51.

Fig. 11. $K^- + p \rightarrow Y^{*+}(1385) + \pi^-$ angular distribution (not normalized).

1.225, 1.375, 1.525, 1.675 BeV/c, Huwe, Ref. 47;

1.450 BeV/c, Cooper et al., Ref. 45;

1.07 BeV/c, Wohl, Refs. 22 and 33.

Fig. 12. $K^- + p \rightarrow Y_1^{*-}(1385) + \pi^+$ angular distribution.

Refs. same as for Fig. 11.

Fig. 13. $K^- + p \rightarrow \Sigma^{\pm} + \pi^{\mp}$ total cross sections.

Refs. 23, 36, 41, 46, 48, 52-54.

Fig. 14. $K^- + p \rightarrow \Sigma^+ + \pi^-$ angular distribution.

3.5 BeV/c, Blair et al., Ref. 41;

3.0 BeV/c, Gelsema et al., Ref. 46;

1.47 BeV/c, Cooper et al., Ref. 53;

1.15 BeV/c, Graziano and Wojcicki, Ref. 23.

See also Appendix A7.

Fig. 15. $K^- + p \rightarrow \Sigma^- + \pi^+$ angular distribution.

Refs. same as for Fig. 14.

Fig. 16. $K^- + p \rightarrow p + (K^{*-} \rightarrow \bar{K}^0 + \pi^-)$ total cross section.

Refs. 39, 46, 49, 55-57.

● - $0.75 \times \sigma(K^- p - \bar{K}^0 \pi^- p)$ Wojcicki UCRL-11138

× - $0.40 \times \sigma(K^- p - \bar{K}^0 \pi^- p)$ Gelsema et al.

○ - $0.30 \times \sigma(\bar{K}^0 \pi^- p)_{\text{lower limit}}$ Bertanza et al.

△ - Alston et al.

□ - $0.75 \times \sigma(K^- p - \bar{K}^0 \pi^- p)$ Gelsema et al.

Fig. 17. $K^- + p \rightarrow K^{*-} + p$ angular distribution.

Refs. 56, 57.

Fig. 18. $K^- + p \rightarrow \Lambda + (\phi \rightarrow K^+K^- + K_1K_2)$ total cross section.

Refs. 41, 43, 58, 59.

Fig. 19. $K^- + p \rightarrow \Lambda + \phi$ angular distributions.

Refs. same as for Fig. 18.

Fig. 20. $K^- + p \rightarrow \Lambda + \rho$ total cross section.

Refs. 46, 47.

Fig. 21. $K^- + p \rightarrow \Lambda + (\omega \rightarrow 3\pi)$ total cross section.

3.0 BeV/c, Gelsema et al., Ref. 46,

2.24 BeV/c, Connolly et al., Ref. 58,

1.2 to 1.7 BeV/c, Flatte et al., Ref. 60.

Fig. 22. $K^- + p \rightarrow \Lambda + \omega$ differential cross section.

Ref. 60.

Fig. 23. $K^- + p \rightarrow \Lambda +$ (neutrals), $(MM)^2$ distribution

Ref. 65.

Fig. 24. $K^- + p \rightarrow \Lambda + \pi^0$ total cross section.

Refs. 32, 36, 48, 64, 65.

Fig. 25. $K^- + p \rightarrow \Lambda + \pi^0$ differential cross section.

Refs. 32, 48, 52, 65.

Fig. 26. Λ Polarization in the reaction $K^- + p \rightarrow \Lambda + \pi^0$.

Ref. 65.

Fig. 27. $d\sigma/d\Omega$ and P_Λ of $K^- + p \rightarrow \Lambda + \pi^0$ from 0.62 to 1.03 BeV/c, compared with the simple exchange model. The differential cross section (in $\mu b/sr$) is displayed in the lower portion of each figure, the Λ polarization in the upper portion.

Ref. 65.

Fig. 28. $d\sigma/d\Omega$ and P_Λ of $K^- + p \rightarrow \Lambda + \pi^0$ from 1.09 to 1.32 BeV/c, compared with the simple exchange model. The differential cross section (in μb/sr) is displayed in the lower portion of each figure, the Λ polarization in the upper portion. Ref. 65.

Fig. 29. $d\sigma/d\Omega$ and P_Λ of $K^- + p \rightarrow \Lambda + \pi^0$ from 1.43 to 1.70 BeV/c, compared with the simple exchange model. The differential cross section (in μb/sr) is displayed in the lower portion of each figure, the Λ polarization in the upper portion. Ref. 65.

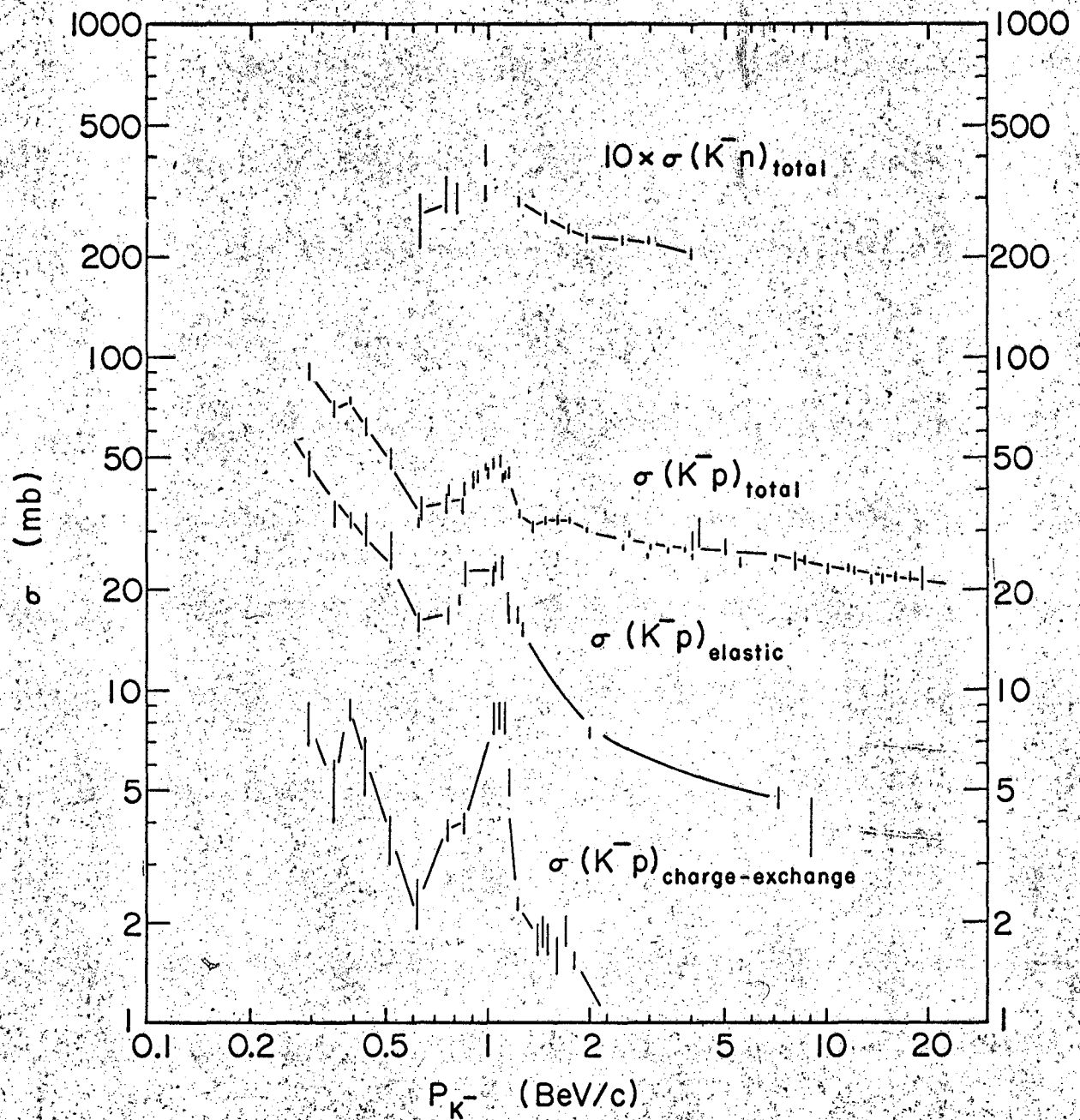
1000
500
200
100
50
20
10
5
2
1
σ (mb)
10 × σ (K⁻n)total
σ (K⁻p)total
σ (K⁻p)elastic
σ (K⁻p)charge-exchange
0.1
0.2
0.5
1
2
5
10
20
P_K⁻ (BeV/c)
MUB-3270

FIG 1

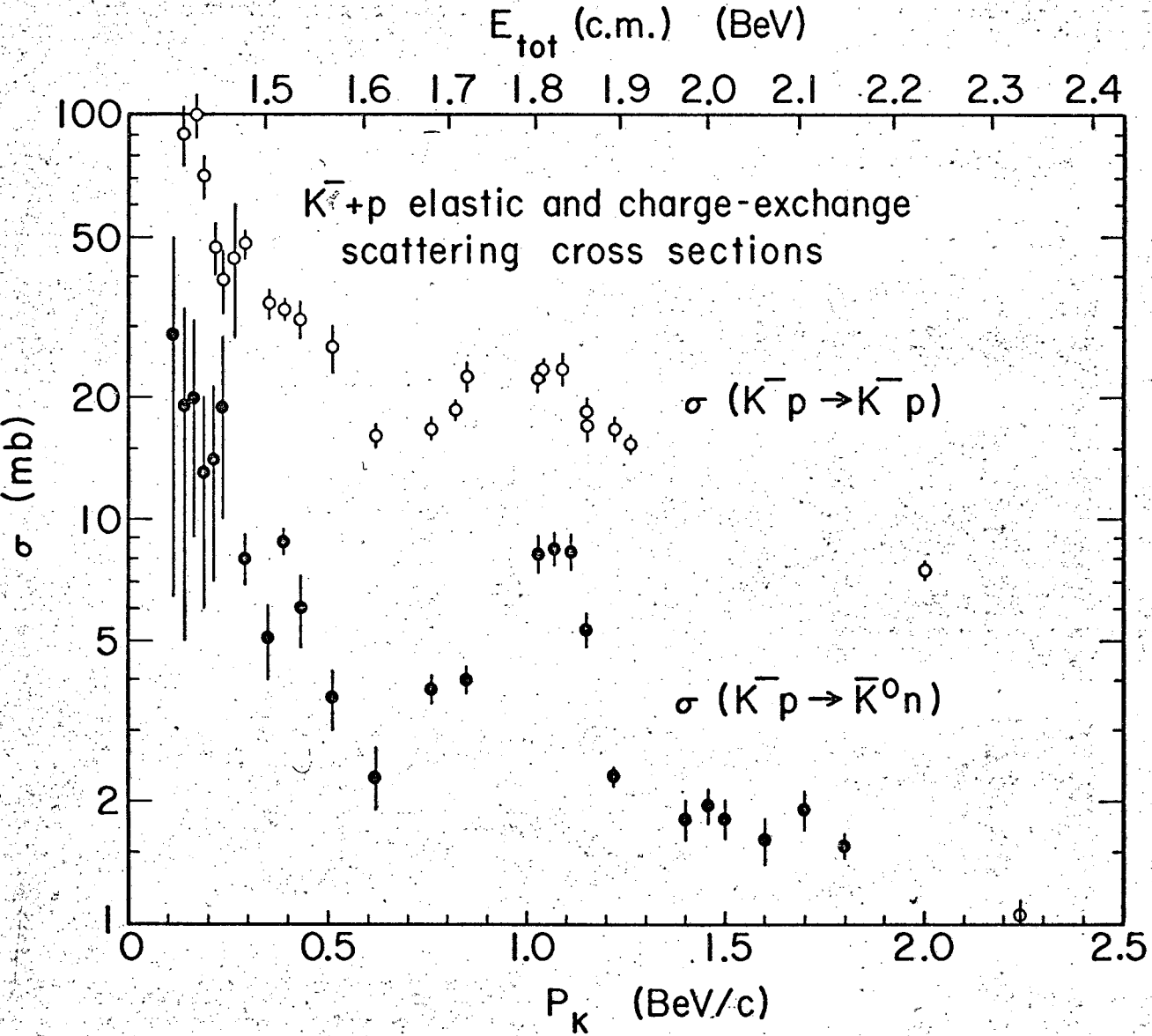

MUB-3271

Fig 2

UCRL-11493

$K^- + p$ Elastic Scattering

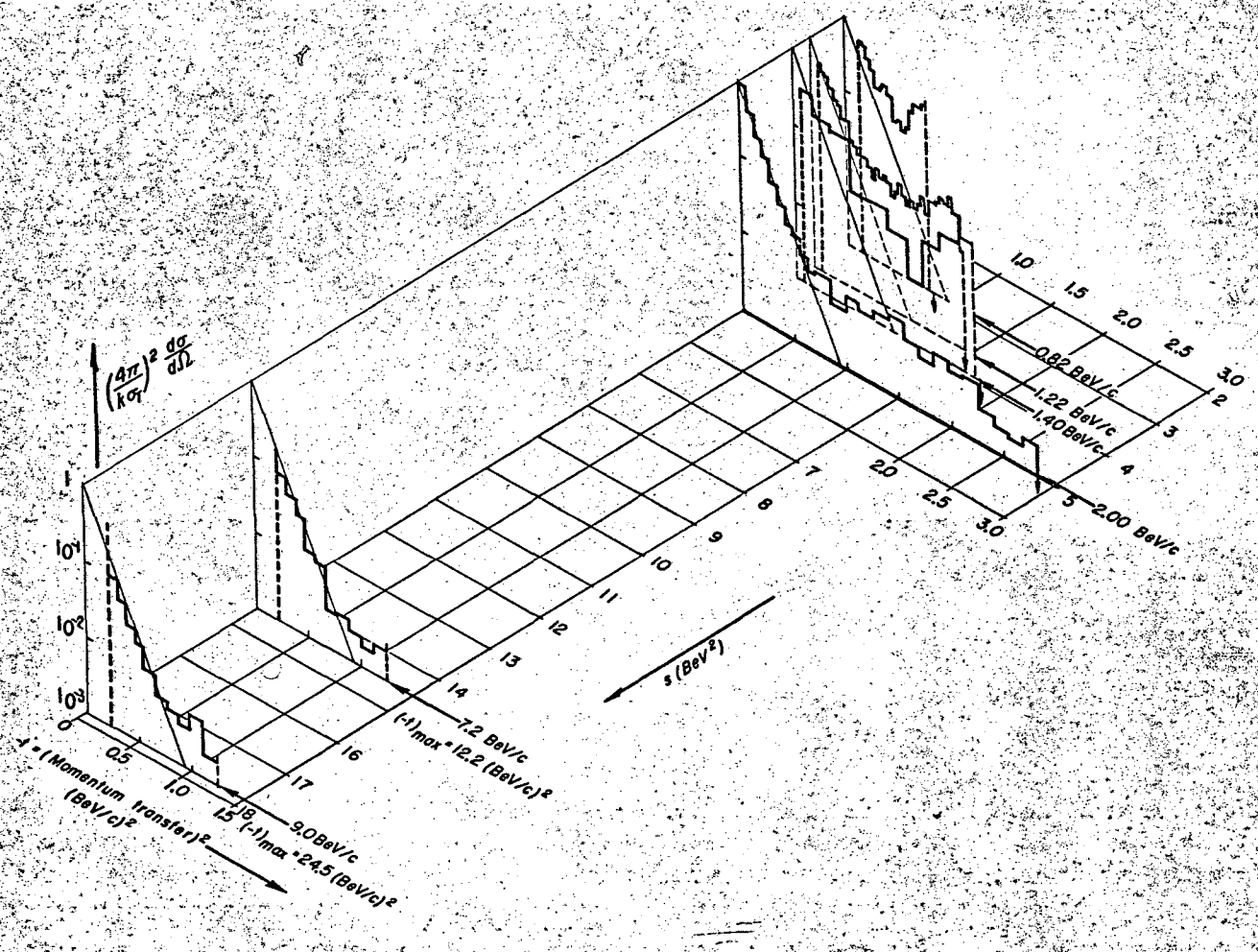

MUB-3276

FIG 3.

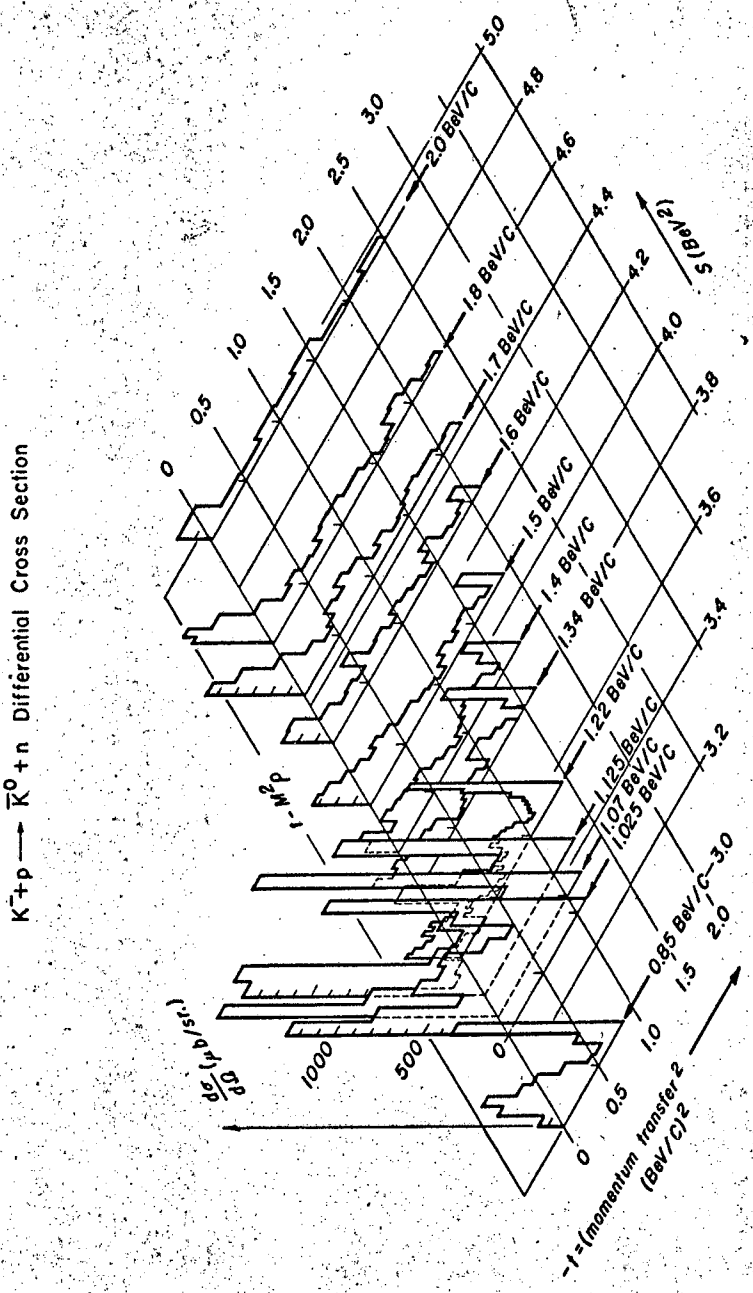

MUB-3277

Fig 4

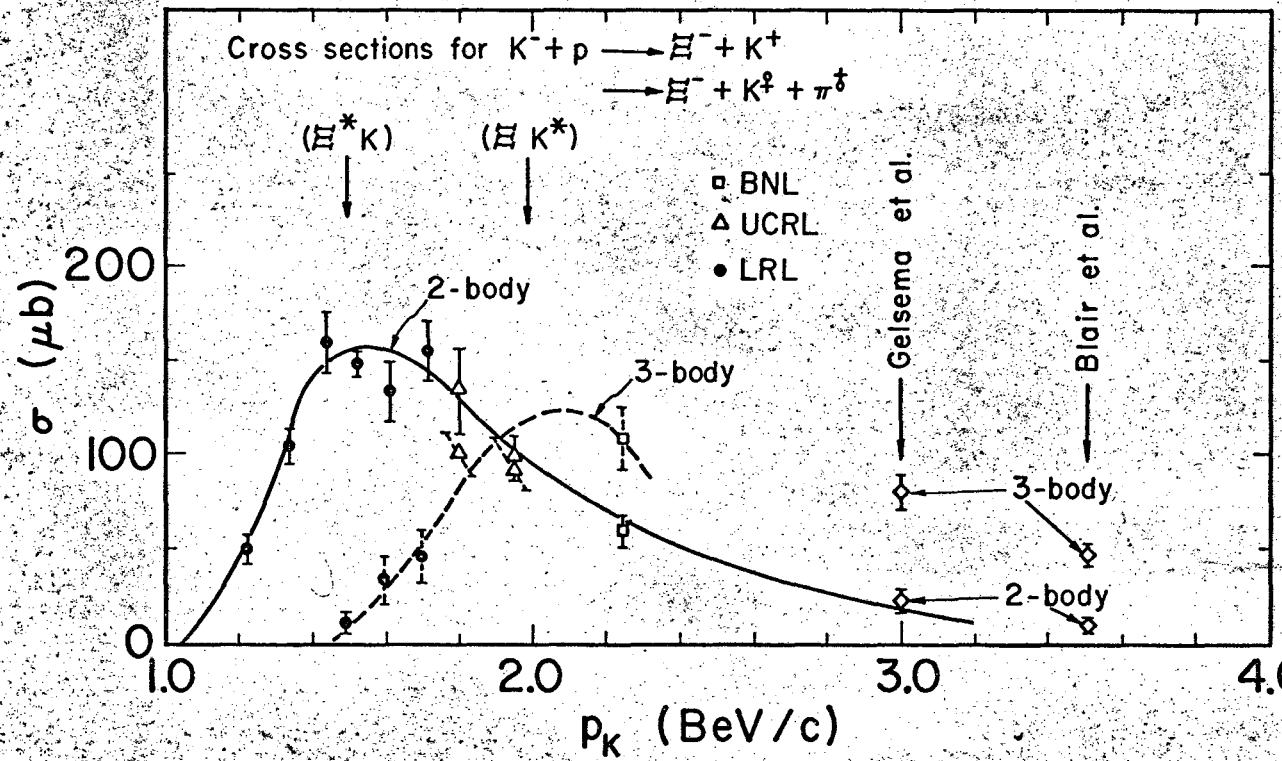

MUB-3262

FIG. 5

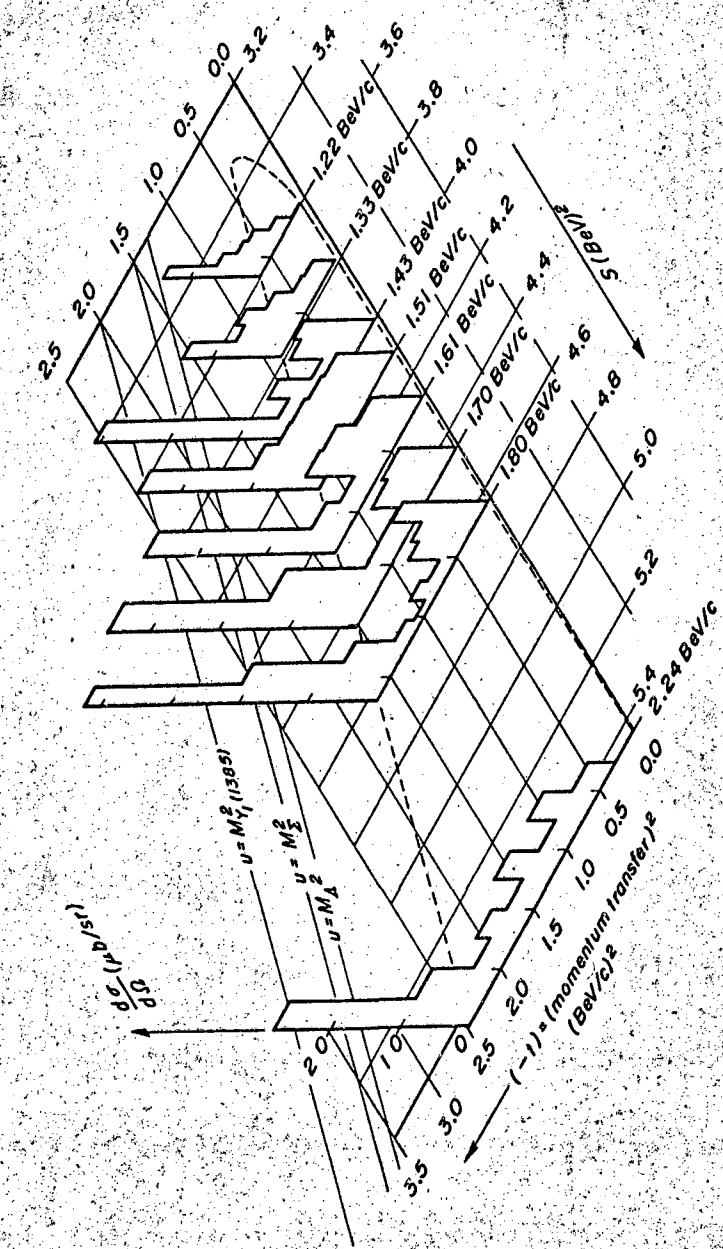

MUB-3461

Fig. 6

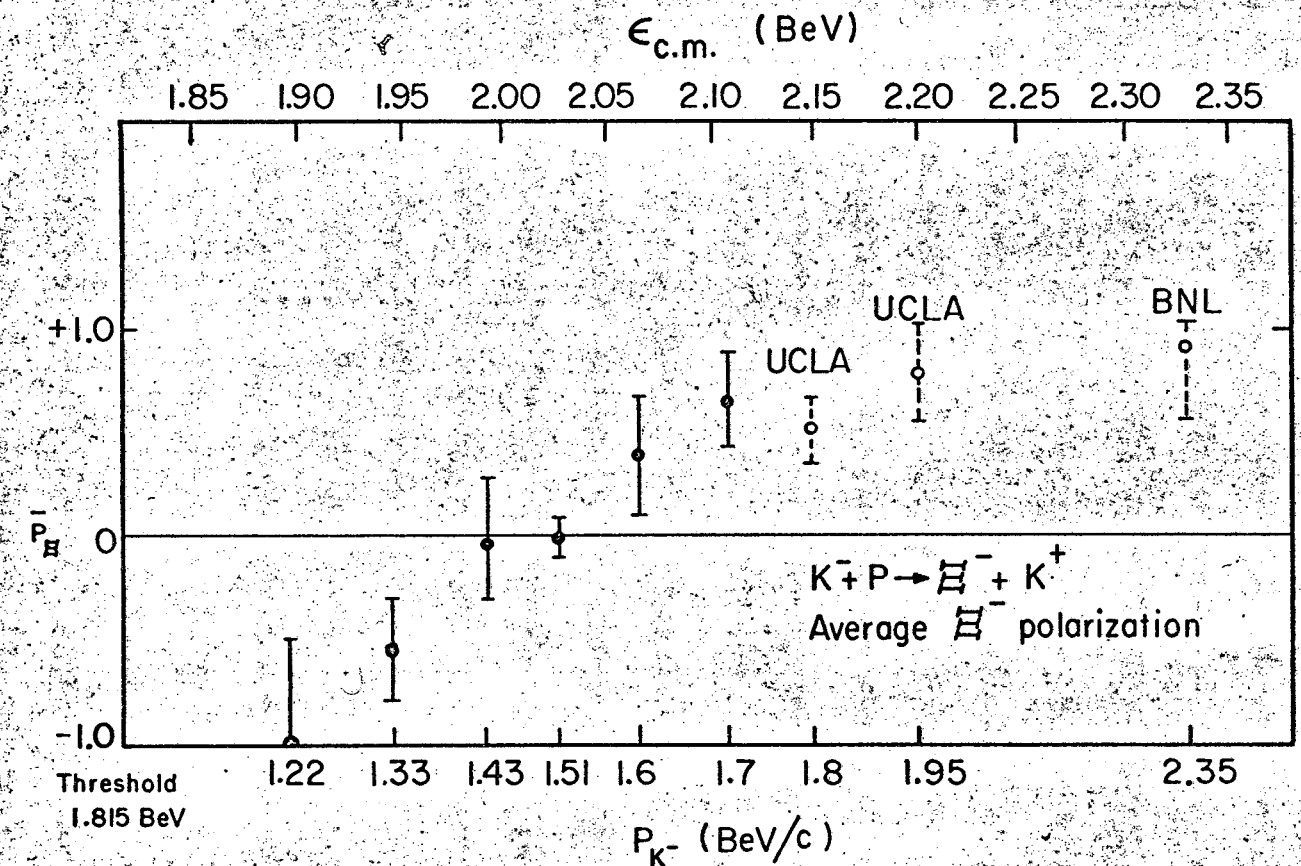

MUB-3269

FIG 7

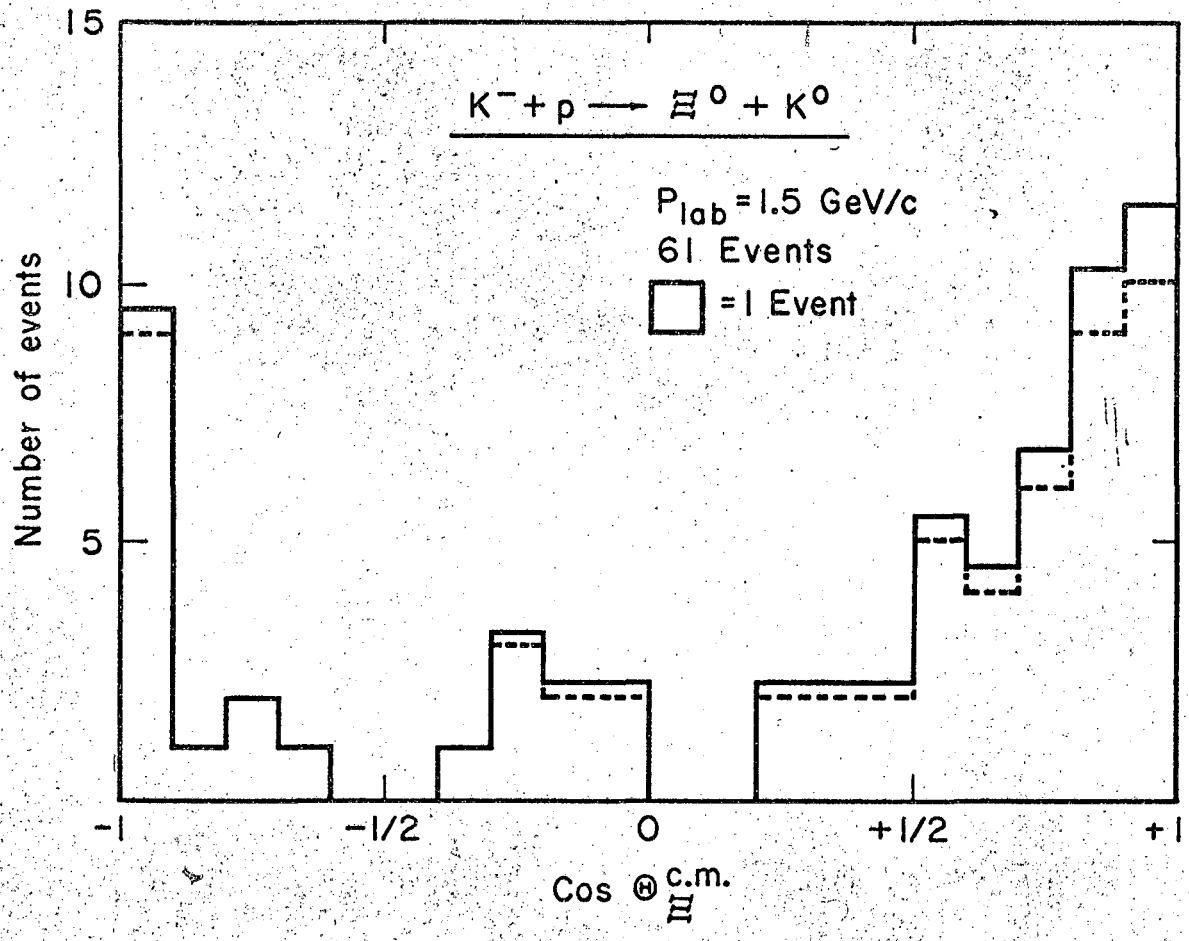

MUB-3260

Fig 8

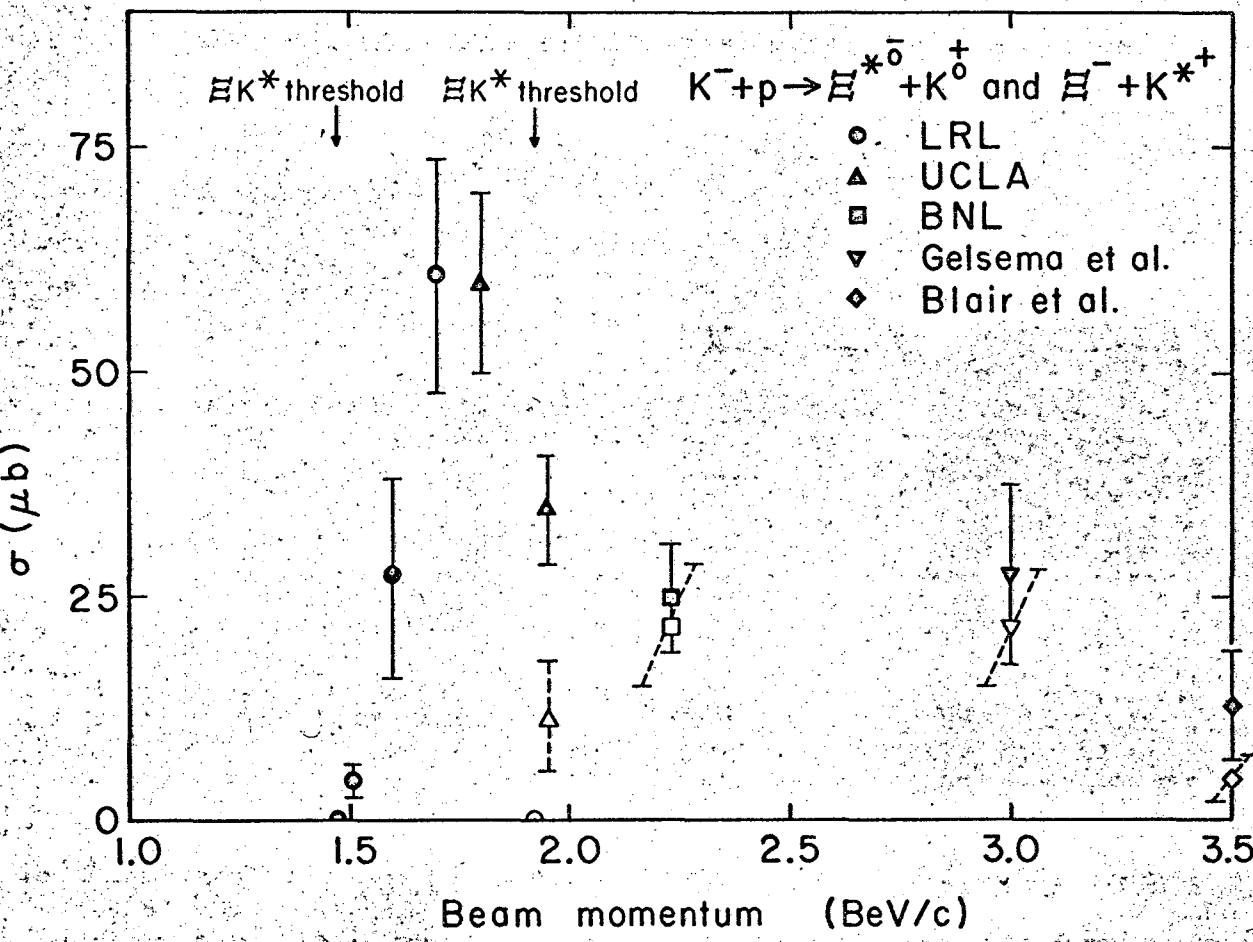

MUB-3491

Fig. 9

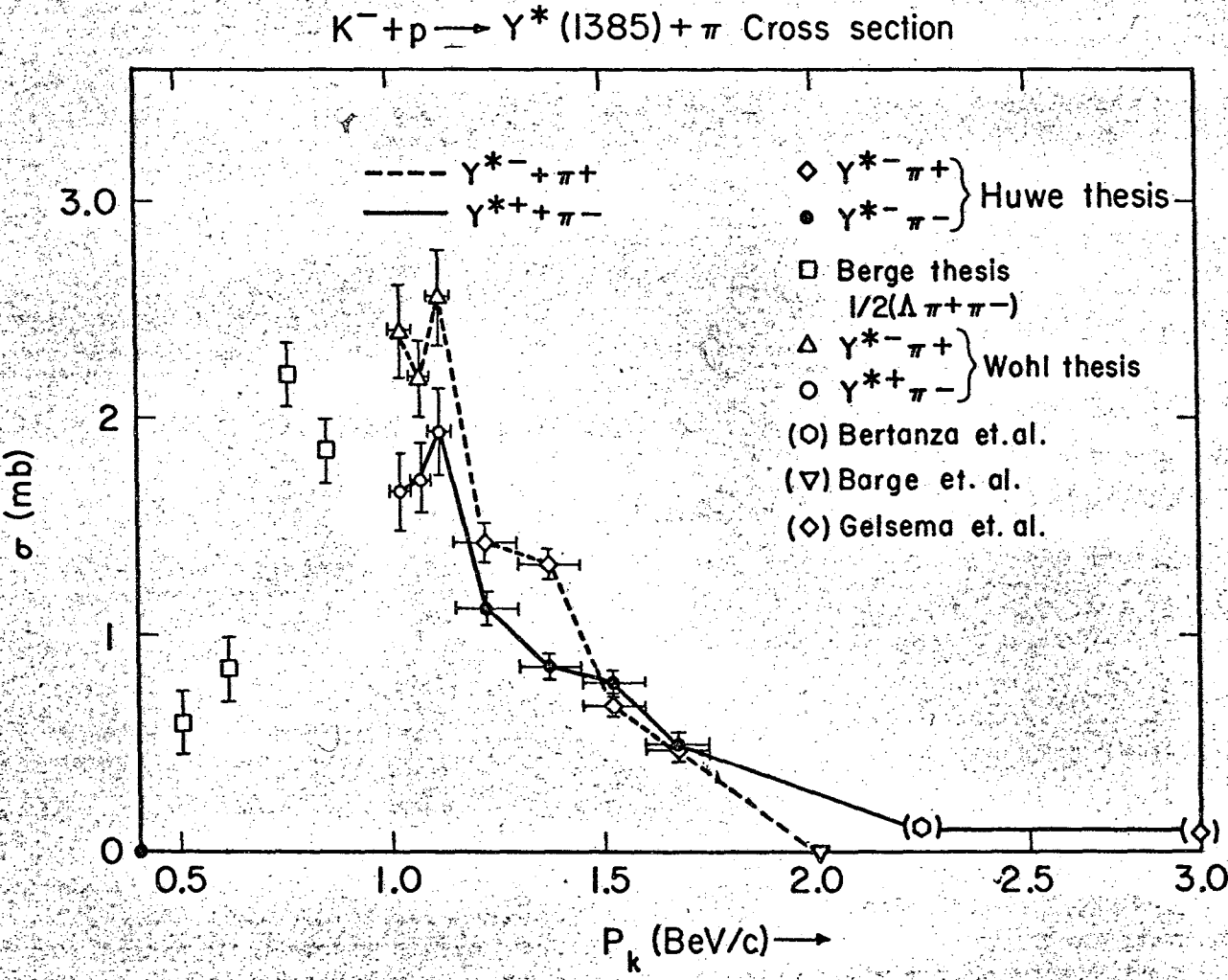

MUB-3265

FIG 10

$K^- p \rightarrow Y_1^+(1385) + \pi^-$ Angular Distribution

(not normalized)

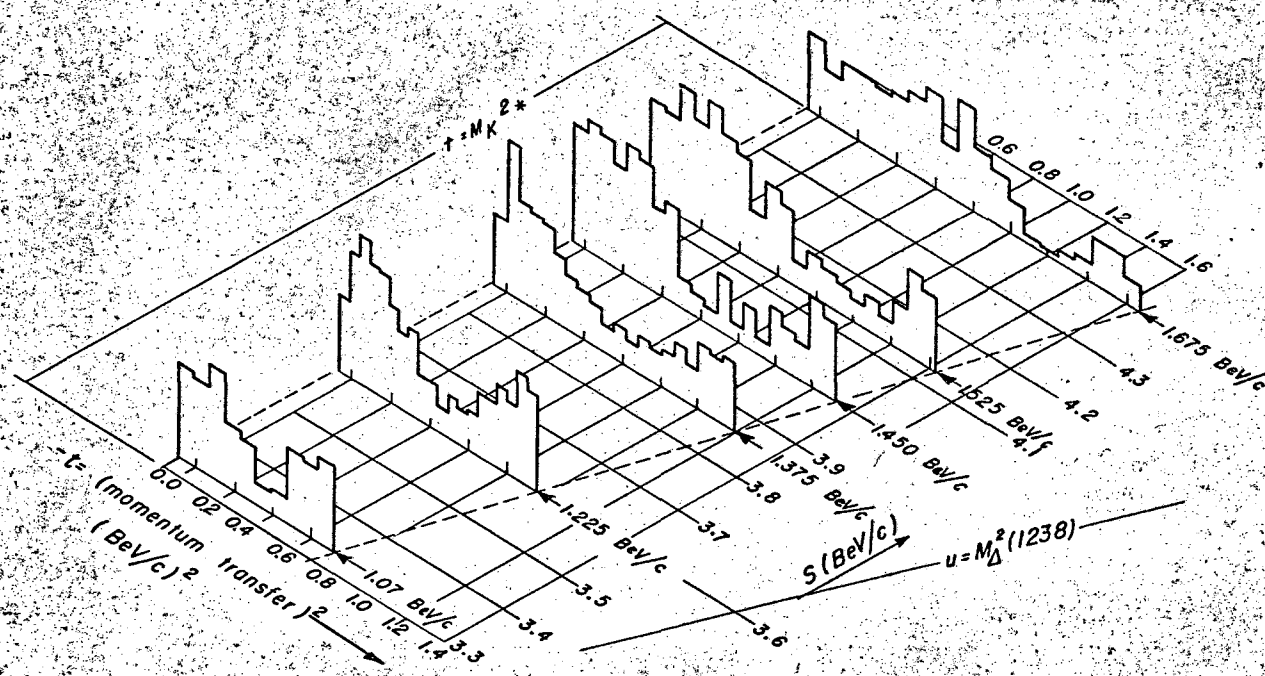

MUB-3288

Fig. 11

UCRL-11493

$K^- + p \rightarrow Y^-(1385) + \pi^+$ Angular Distribution

(Not normalized)

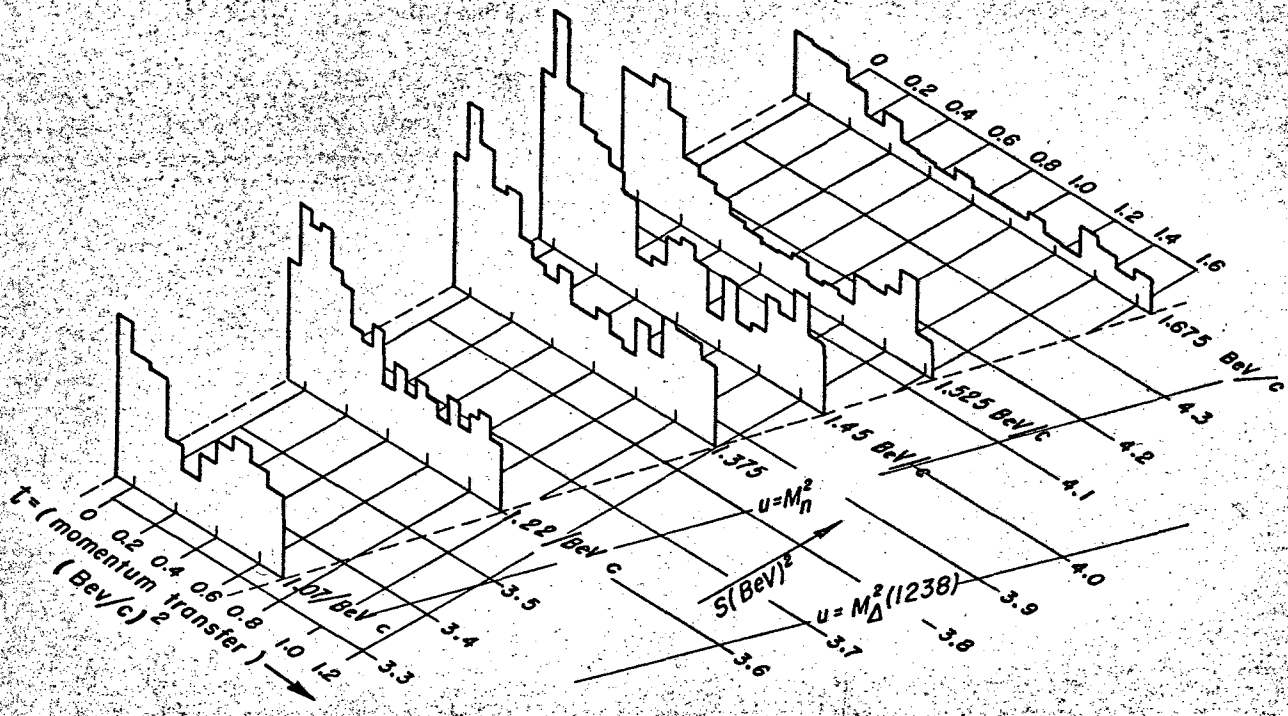

MUB-3275

FIG 12

UCRL-11493

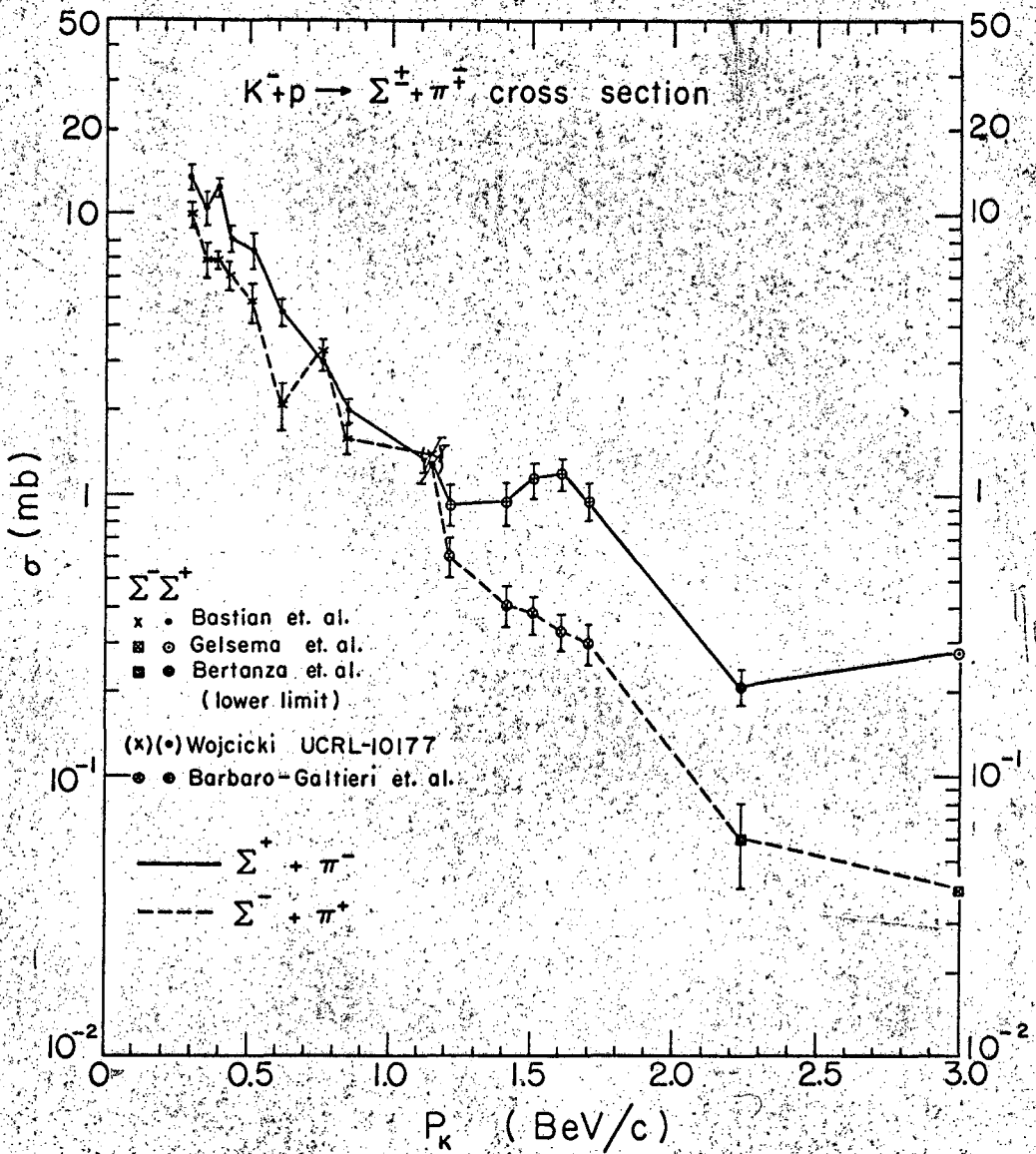
$K^- + p \rightarrow \Sigma^{\pm} + \pi^{\mp}$ cross section
σ (mb)
P_K (BeV/c)
$\Sigma^-\Sigma^+$
x • Bastian et. al.
⊠ ⊙ Gelsema et. al.
■ ● Bertanza et. al.
(lower limit)
(x)(•) Wojcicki UCRL-10177
⊙ ● Barbaro-Galtieri et. al.
$\Sigma^+ + \pi^-$
$\Sigma^- + \pi^+$
MUB-3278

FIG 13

$K^- + p \longrightarrow \Sigma^+ + \pi^-$ Angular Distribution

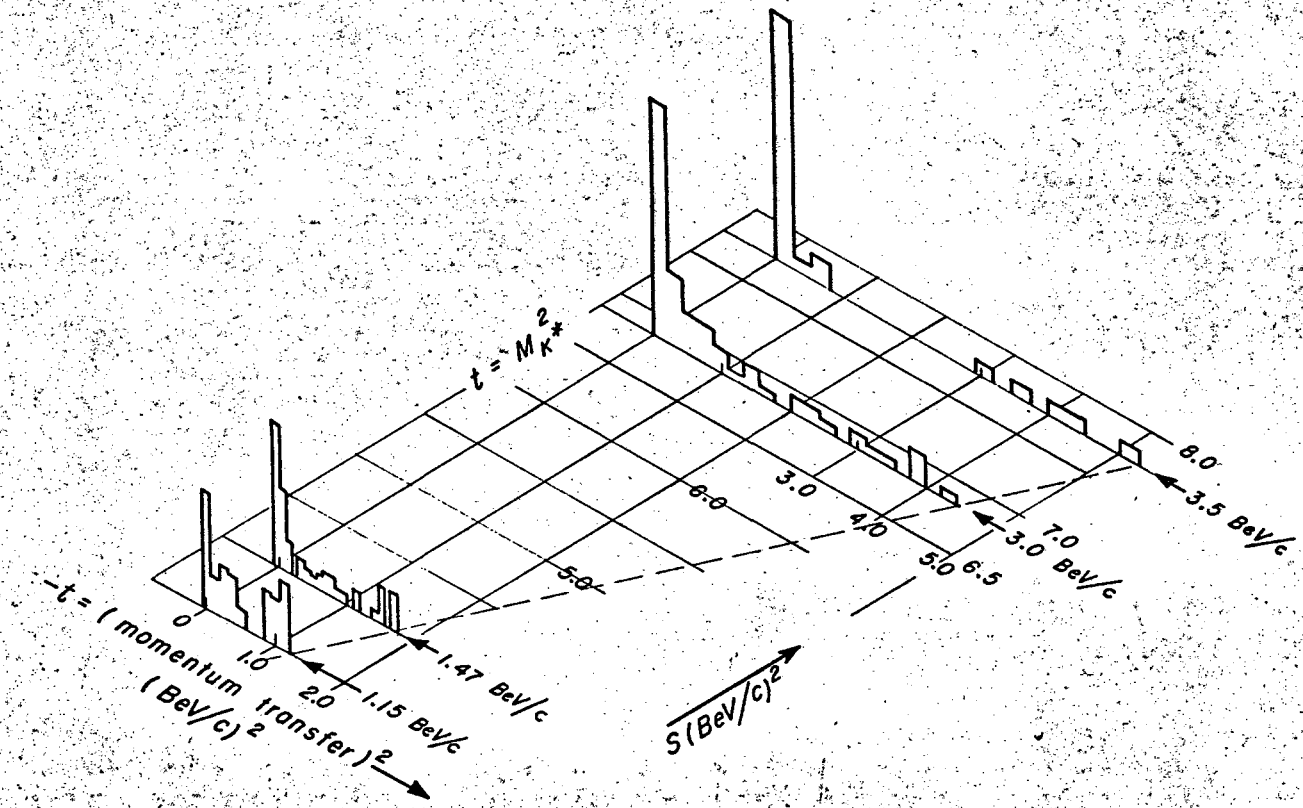

Fig. 14

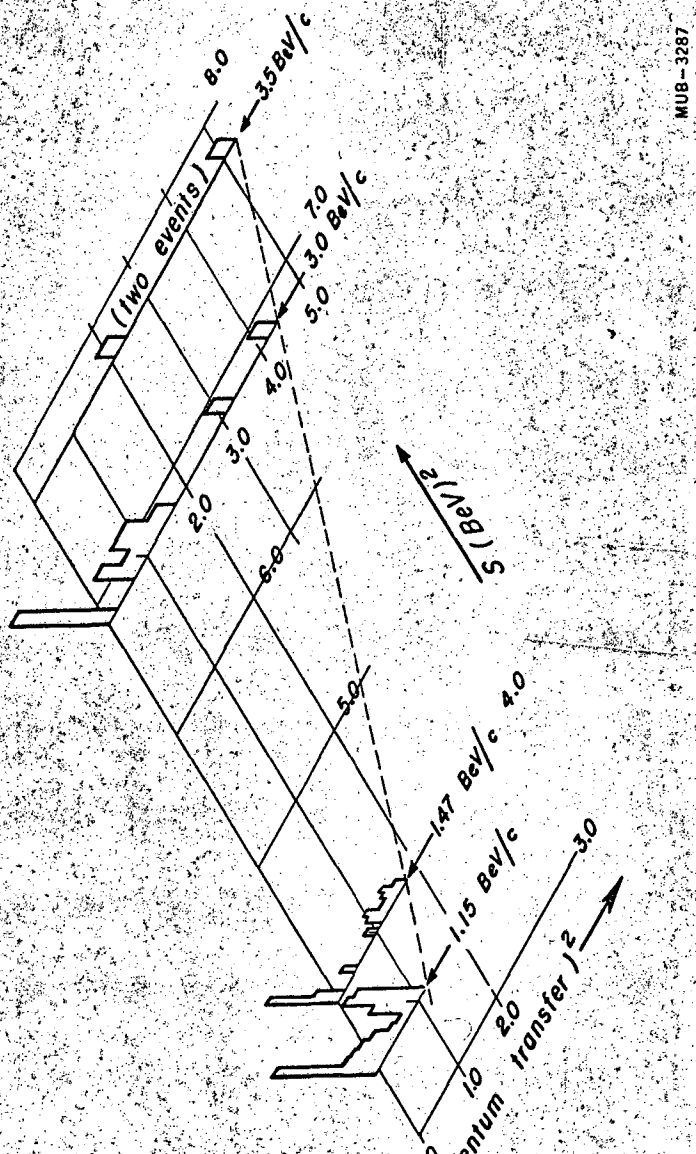
$K^- + p \rightarrow \Sigma^- + \pi^+$ Angular Distribution
8.0
3.5 BeV/c
(two events)
7.0
3.0 BeV/c
5.0
4.0
3.0
2.0
6.0
5.0
S (BeV/c)^2
4.0
1.47 BeV/c
1.15 BeV/c
3.0
2.0
1.0
0
$-t$ = (momentum transfer)^2
MUB-3287

Fig 15

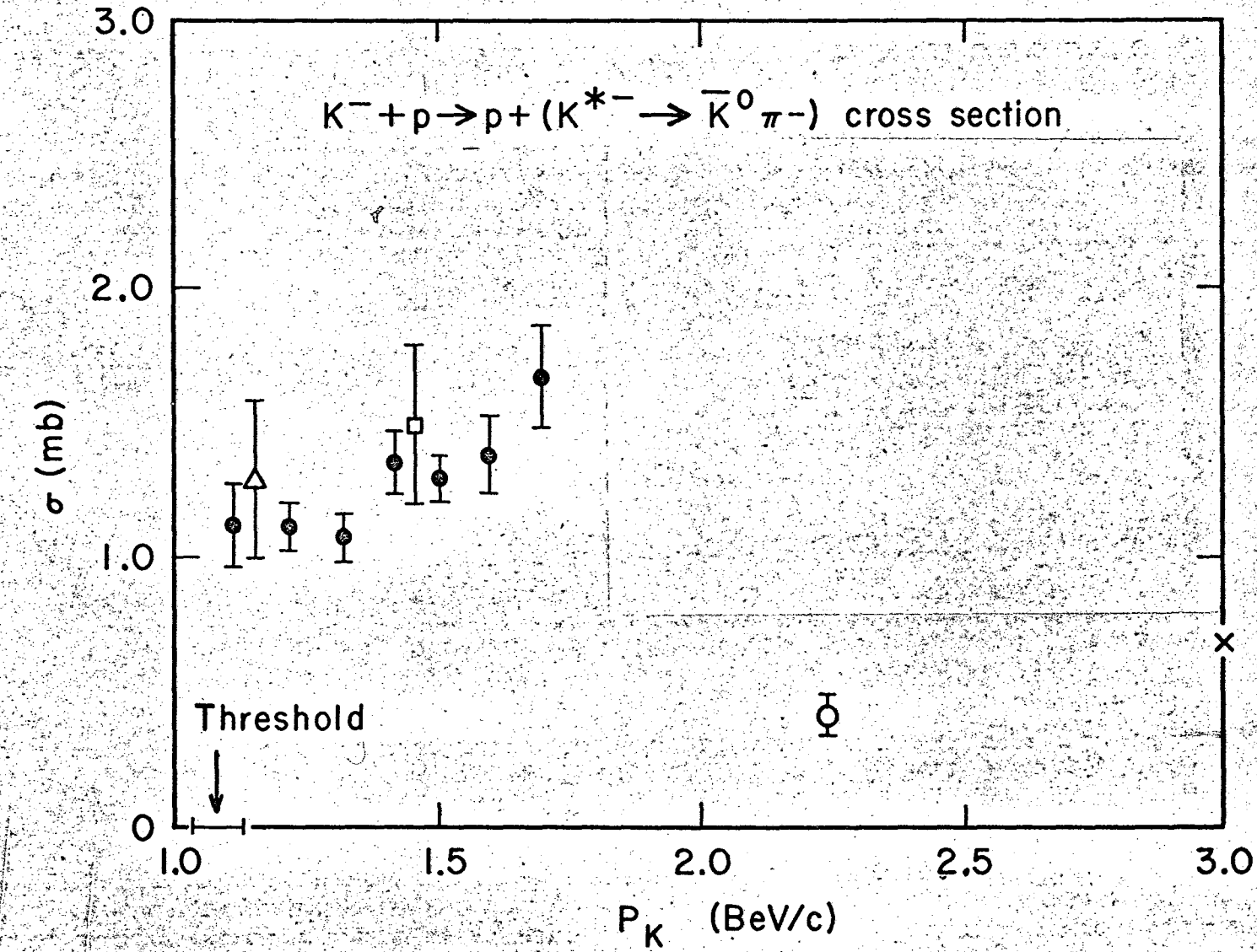

UCRL-11493

MUB-3268

FIG 16

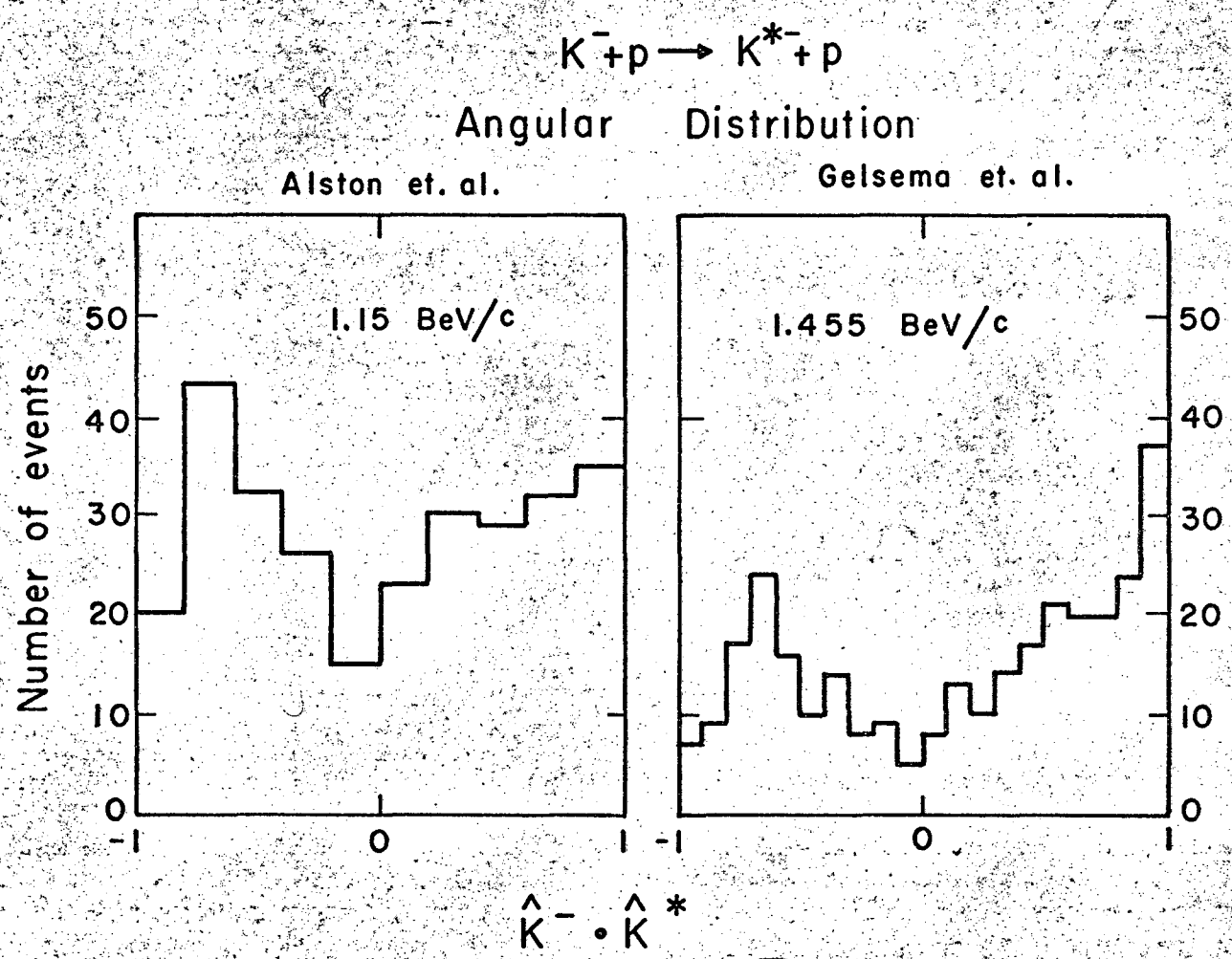

MUB-3286

Fig 17

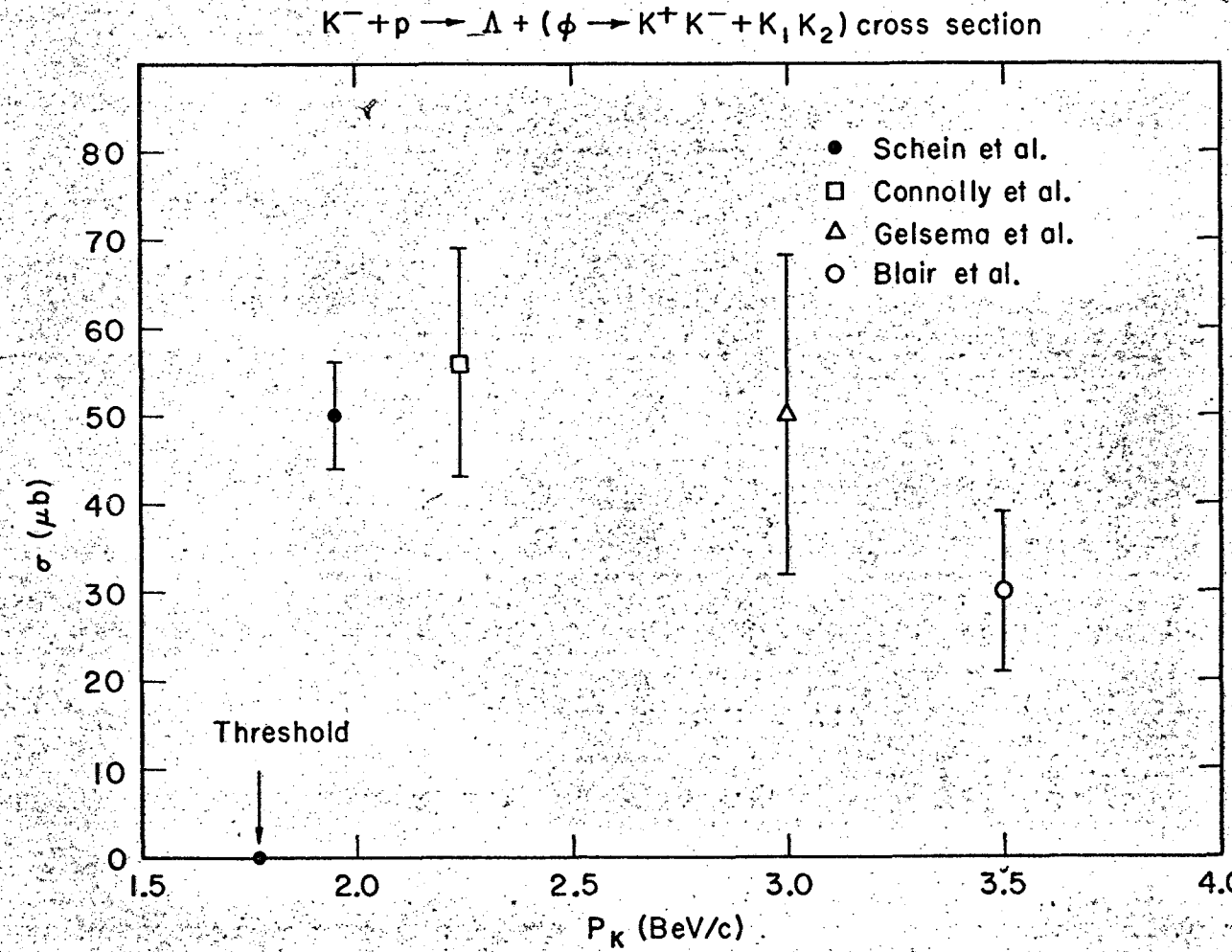

MUB-3264

Fig. 18

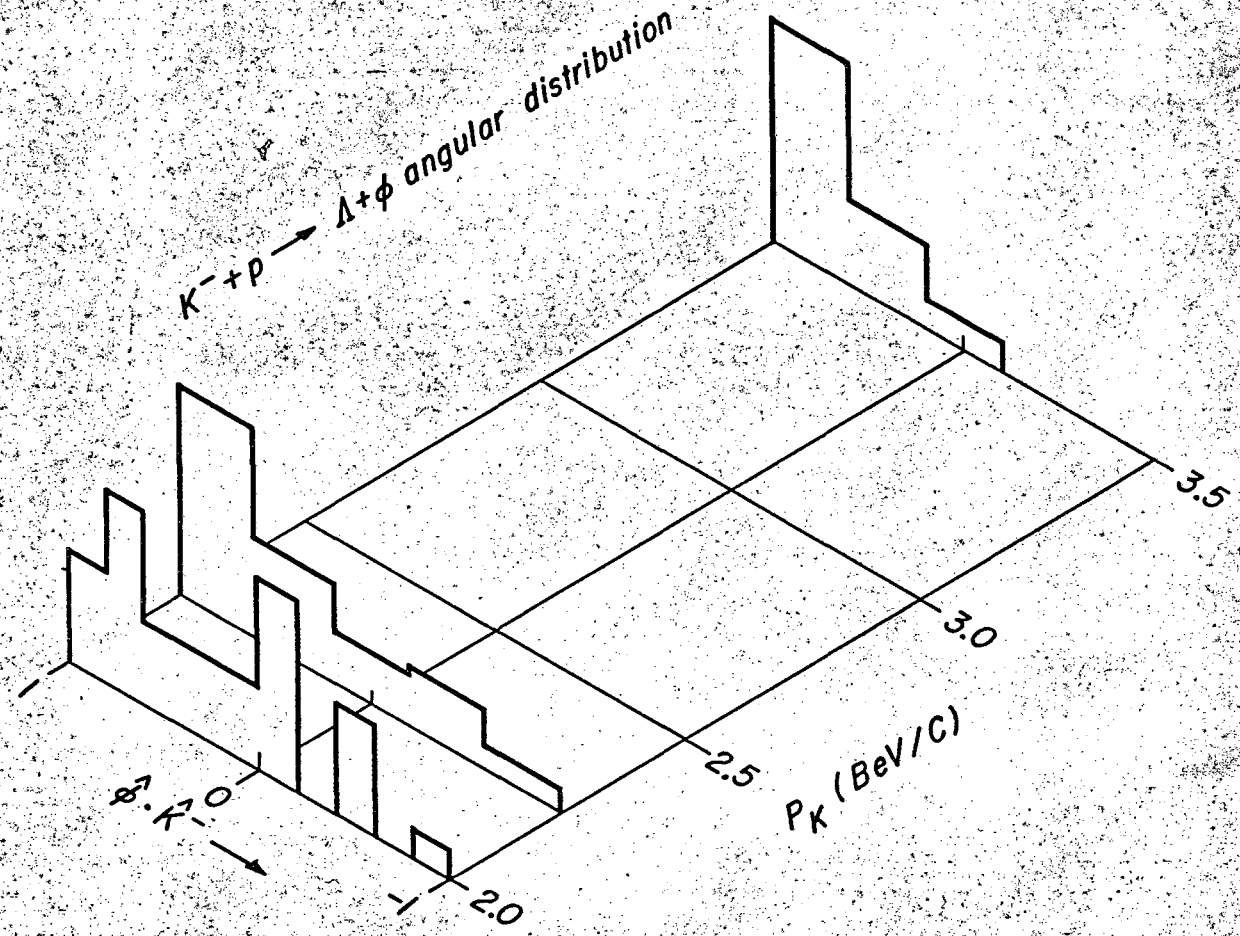

MUB-3266

Fig 19

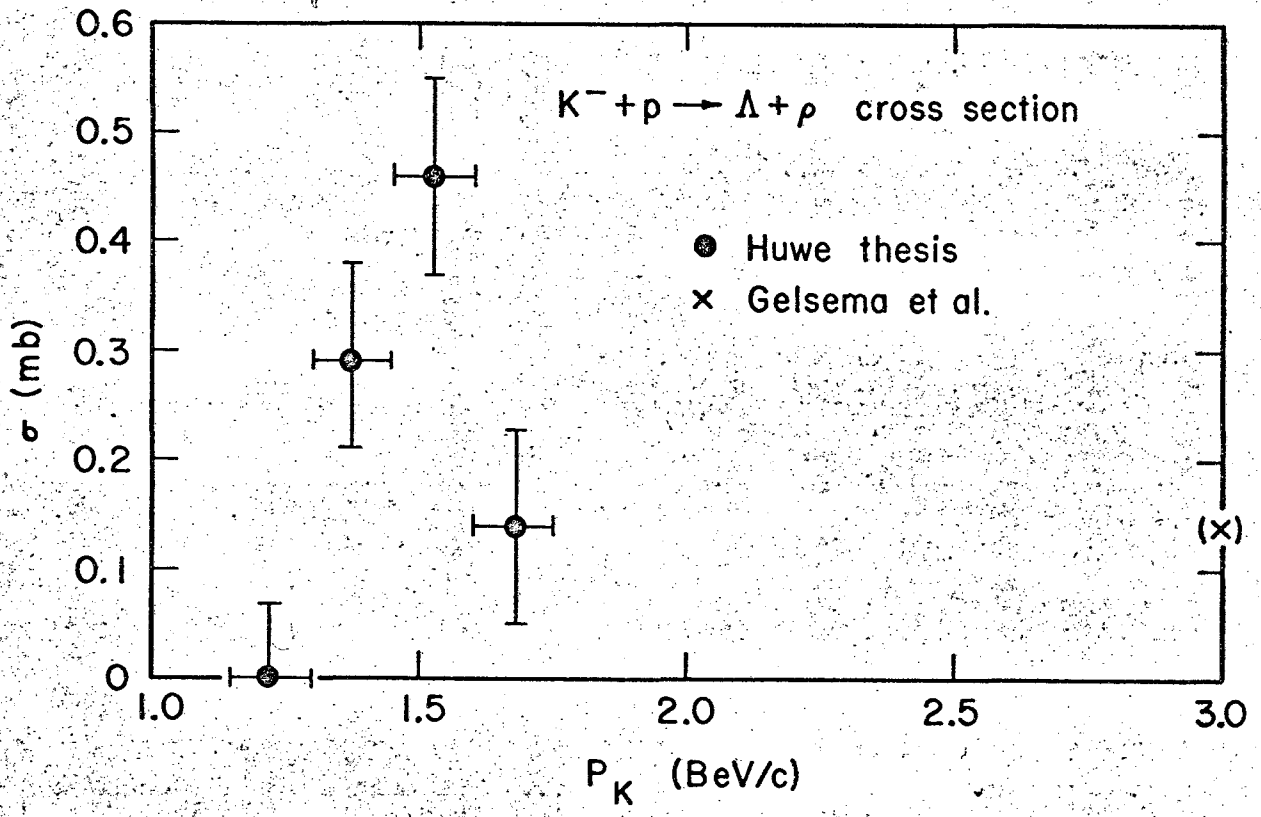

MUB-3267

FIG 20

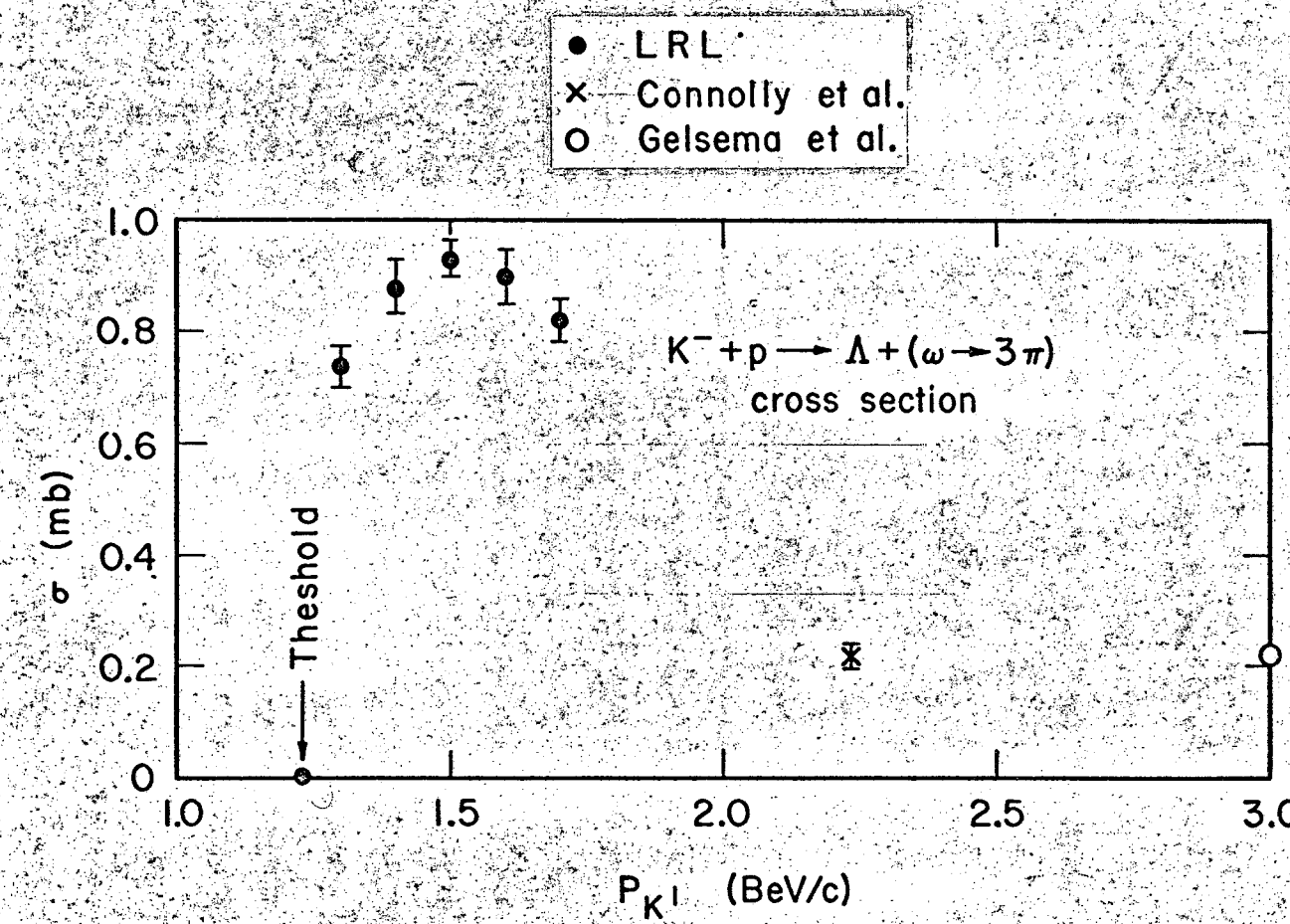

MUB-3261

UCRL-11493

Fig 21

Fig 22

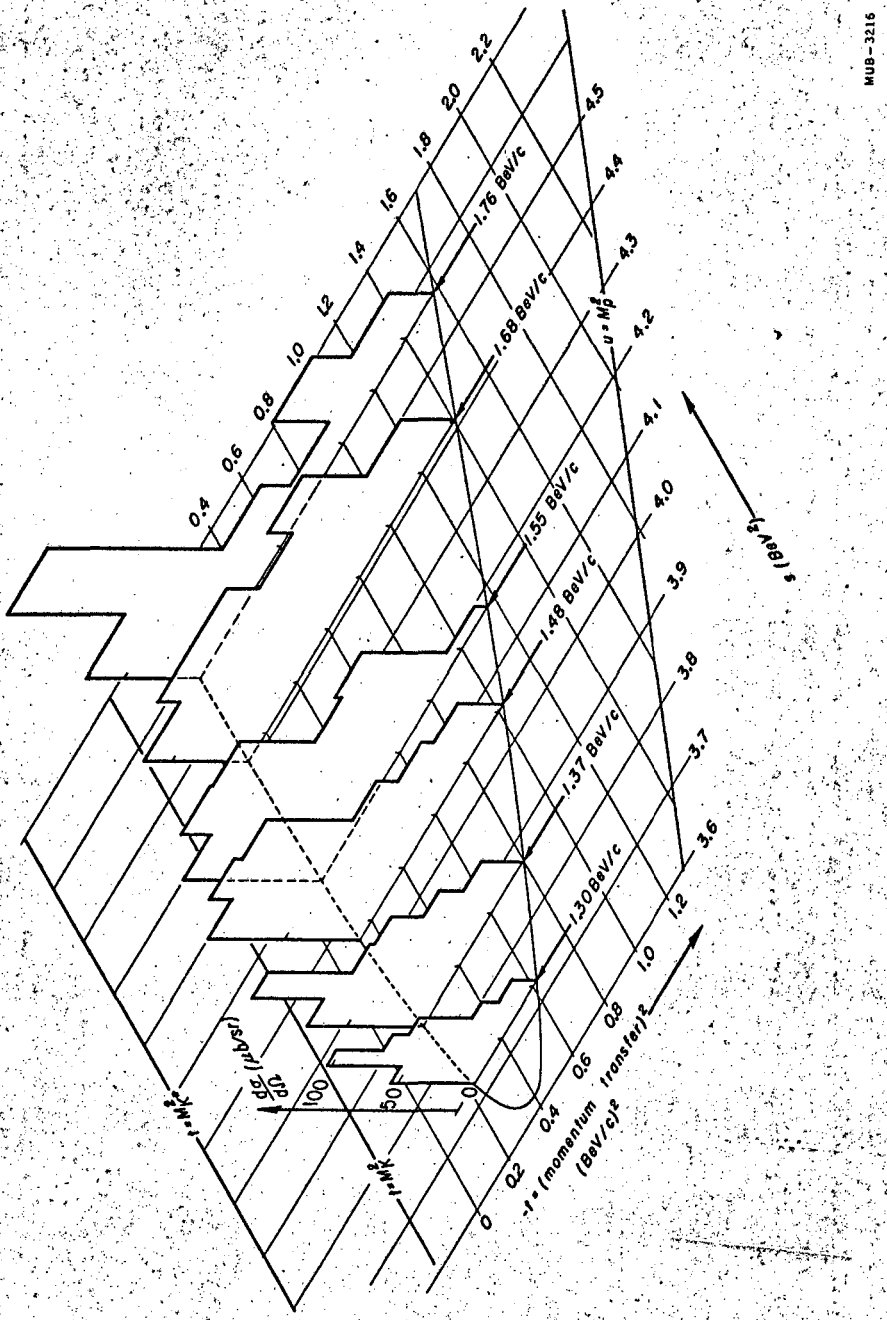
$K^- + p \rightarrow \Lambda + \omega$ Differential Cross Section
MUB-3216
$u = M_p^2$
1.76 BeV/c
1.68 BeV/c
1.55 BeV/c
1.48 BeV/c
1.37 BeV/c
1.30 BeV/c
s (BeV)^2
$t = M_\omega^2$
$u = M_p^2$
$\frac{d\sigma}{dt}$ (μb/sr)
-t (momentum transfer)^2 (BeV/c)^2

Fig 23

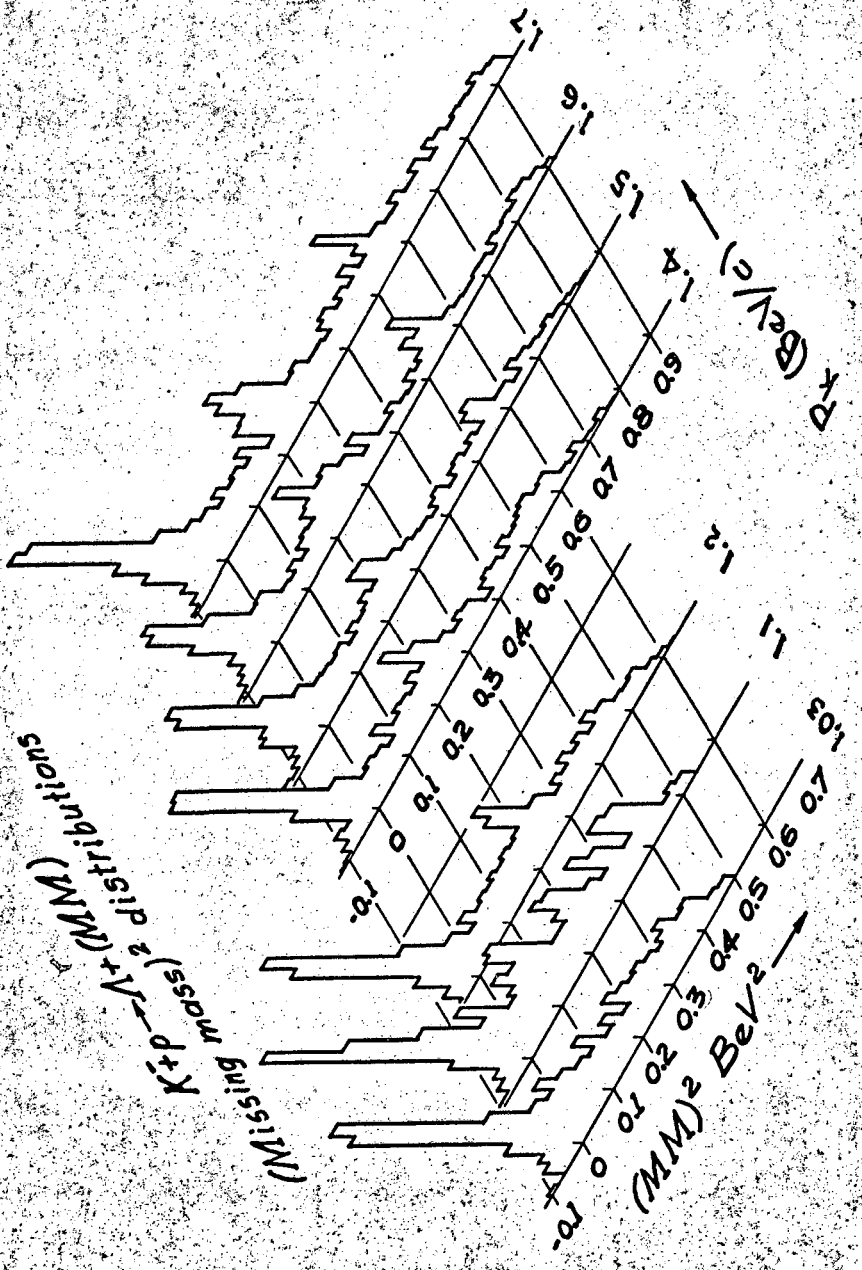

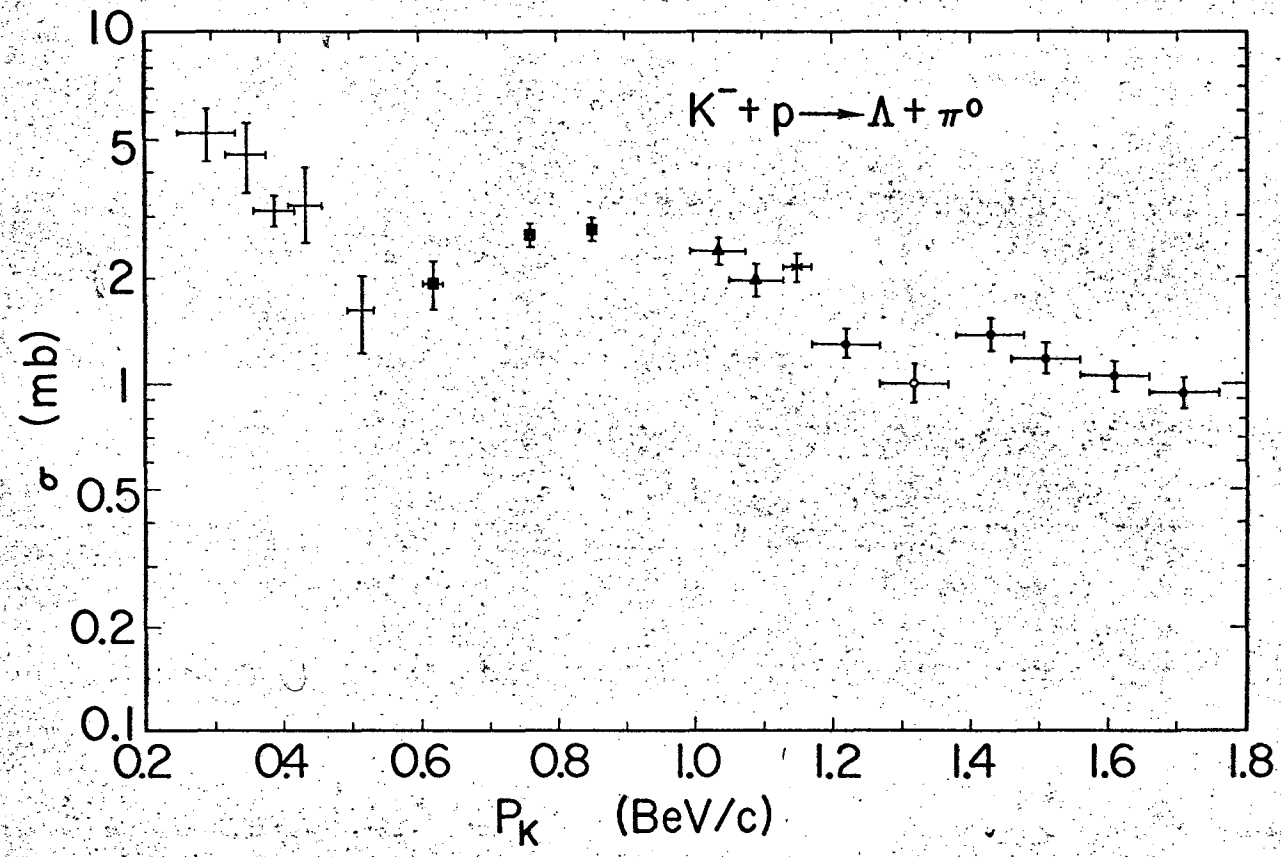

FIG 24

UCRL-11493

$K^- + p \longrightarrow \Lambda + \pi^0$ Differential Cross Section

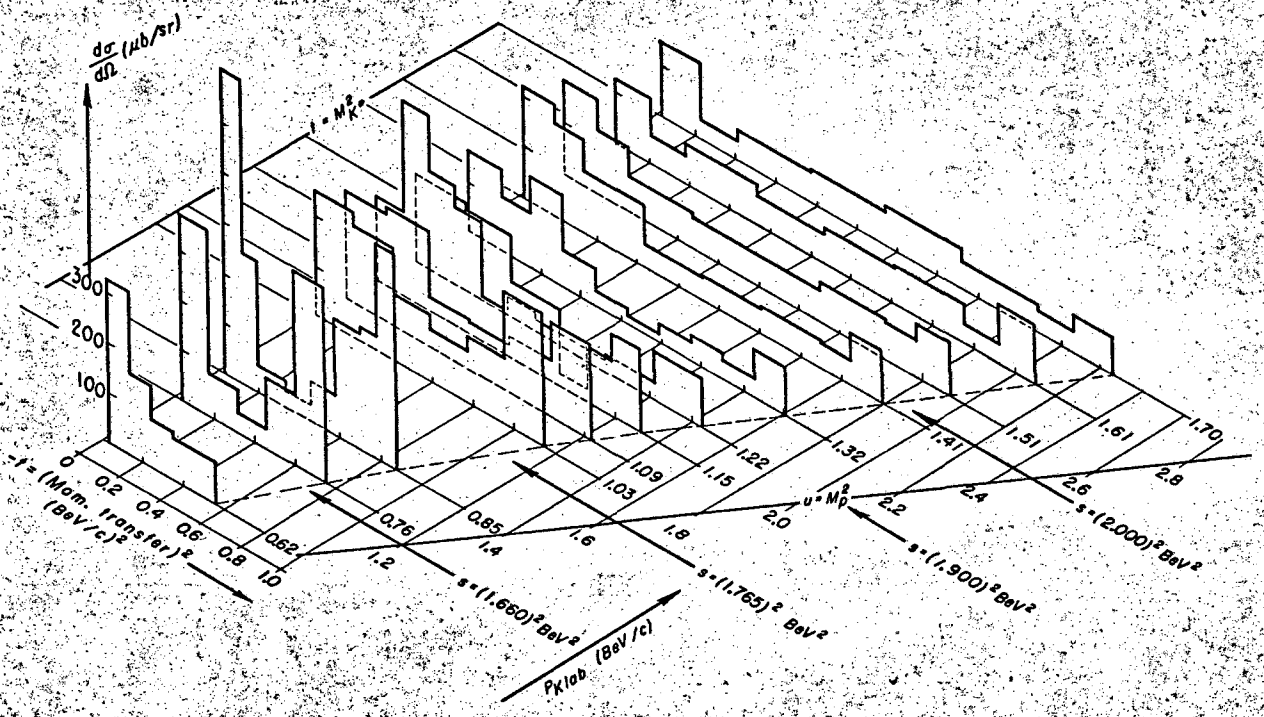

MUB-3206

FIG 25

Fig 26

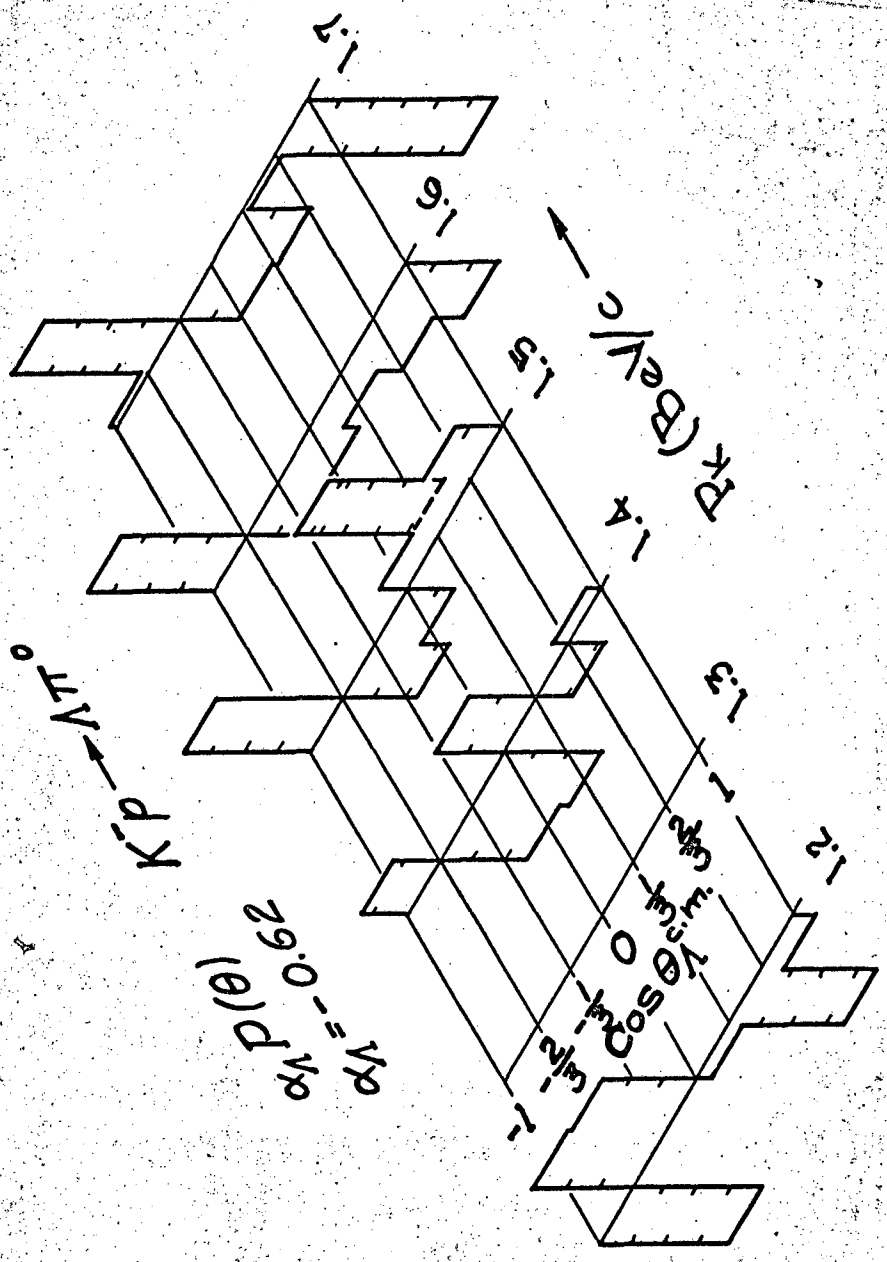

MUB-2580

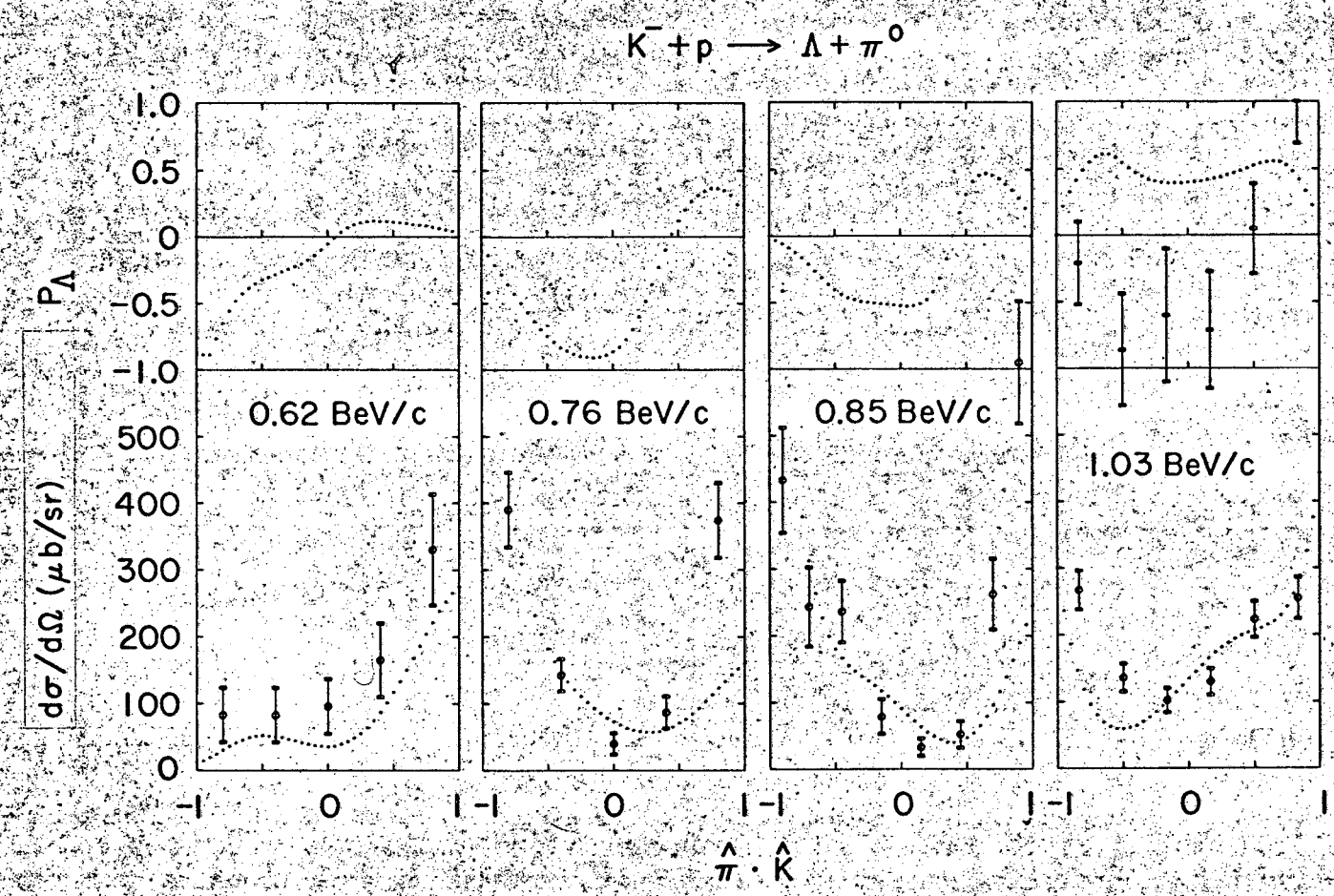

UCRL-11493

Fig 27

$K^- + p \longrightarrow \Lambda + \pi^0$
1.09 BeV/c
1.15 BeV/c
1.22 BeV/c
1.32 BeV/c
P_Λ
$d\sigma/d\Omega$ (μb/sr)
$\hat{\pi} \cdot \hat{K}$

Fig 24

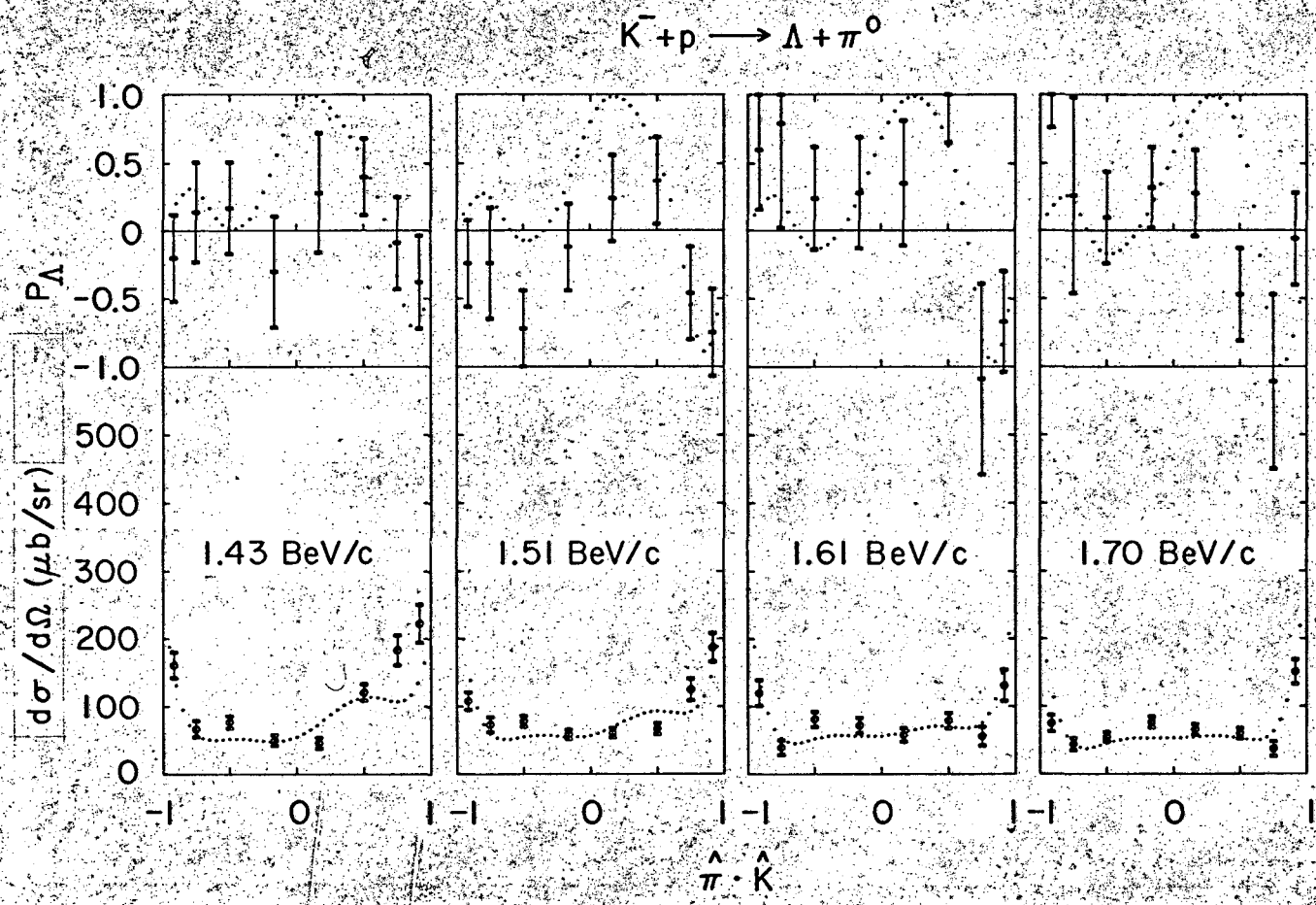
$K^- + p \longrightarrow \Lambda + \pi^0$
P_Λ
$d\sigma/d\Omega$ (μb/sr)
1.0
0.5
0
-0.5
-1.0
500
400
300
200
100
0
1.43 BeV/c
1.51 BeV/c
1.61 BeV/c
1.70 BeV/c
-1
0
1
$\hat{\pi} \cdot \hat{K}$

Fig 29